






Article

Inducing Angiogenesis in the Nucleus Pulposus

Sheela R. Damle ¹, Agata K. Krzyzanowska ¹, Maximilian K. Korsun ¹, Kyle W. Morse ¹, Susannah Gilbert ¹, Han Jo Kim ^{1,2}, Oheneba Boachie-Adjei ^{1,2}, Bernard A. Rawlins ^{1,2}, Marjolein C. H. van der Meulen ^{1,3}, Matthew B. Greenblatt ², Chisa Hidaka ^{1,4} and Matthew E. Cunningham ^{1,2,*}

¹ HSS Research Institute, Hospital for Special Surgery, 515 E 71st Street, New York, NY 10021, USA

² Weill Cornell Medical College, Cornell University, New York, NY 10065, USA

³ Meinig School of Biomedical Engineering and Sibley School of Mechanical & Aerospace Engineering, Cornell University, Ithaca, NY 14853, USA

⁴ Department of Genetic Medicine and Belfer Gene Therapy Core Facility, Weill Medical College of Cornell University, New York, NY 10065, USA

* Correspondence: cunningham@hss.edu

Abstract: Bone morphogenetic protein (BMP) gene delivery to Lewis rat lumbar intervertebral discs (IVDs) drives bone formation anterior and external to the IVD, suggesting the IVD is inhospitable to osteogenesis. This study was designed to determine if IVD destruction with a proteoglycanase, and/or generating an IVD blood supply by gene delivery of an angiogenic growth factor, could render the IVD permissive to intra-discal BMP-driven osteogenesis and fusion. Surgical intra-discal delivery of naïve or gene-programmed cells (BMP2/BMP7 co-expressing or VEGF₁₆₅ expressing) +/- purified chondroitinase-ABC (chABC) in all permutations was performed between lumbar 4/5 and L5/6 vertebrae, and radiographic, histology, and biomechanics endpoints were collected. Follow-up anti-sFlt Western blotting was performed. BMP and VEGF/BMP treatments had the highest stiffness, bone production and fusion. Bone was induced anterior to the IVD, and was not intra-discal from any treatment. chABC impaired BMP-driven osteogenesis, decreased histological staining for IVD proteoglycans, and made the IVD permissive to angiogenesis. A soluble fragment of VEGF Receptor-1 (sFlt) was liberated from the IVD matrix by incubation with chABC, suggesting dysregulation of the sFlt matrix attachment is a possible mechanism for the chABC-mediated IVD angiogenesis we observed. Based on these results, the IVD can be manipulated to foster vascular invasion, and by extension, possibly osteogenesis.

Keywords: intervertebral disc; angiogenesis; osteogenesis; fusion; gene delivery; proteoglycanase nucleus pulposus



Citation: Damle, S.R.; Krzyzanowska, A.K.; Korsun, M.K.; Morse, K.W.; Gilbert, S.; Kim, H.J.; Boachie-Adjei, O.; Rawlins, B.A.; van der Meulen, M.C.H.; Greenblatt, M.B.; et al. Inducing Angiogenesis in the Nucleus Pulposus. *Cells* **2023**, *12*, 2488. <https://doi.org/10.3390/cells12202488>

Academic Editor: Hideki Sudo

Received: 31 July 2023

Revised: 22 September 2023

Accepted: 26 September 2023

Published: 19 October 2023



Copyright: © 2023 by the authors. Licensee MDPI, Basel, Switzerland. This article is an open access article distributed under the terms and conditions of the Creative Commons Attribution (CC BY) license (<https://creativecommons.org/licenses/by/4.0/>).

1. Introduction

Patients experiencing intolerable axial spine pain refractory to non-operative treatment, either in the setting of *spinal instability* (hypermobility due to fracture, spondylolisthesis, or end-stage spondylosis), regional *spinal deformity* (scoliosis, kyphosis), or certain *spinal infections/neoplastic* diagnoses, are frequently indicated for segmental spinal fusions as definitive treatment. Fusion of the affected spinal segments limits or eliminates axial pain by stabilizing treated hypermobile segments, by correcting current and preventing progressive spinal deformity, and by augmenting structural integrity of the spine in situations of impending pathological fractures. The current surgical technique includes using metal implants to immobilize the spinal vertebrae to be fused, decortication of strategic surfaces of the vertebrae to increase osteoprogenitor cell populations in the intended fusion site and to induce local osteogenesis mechanisms, and placement of bone grafts to optimize osteoconduction and osteoinduction. The expectation is that a non-mineralized osteoid anlage is generated, the anlage evolves and undergoes mineralization forming a mature bone fusion mass, and that as the anlage evolves/mineralizes, the spine progressively stiffens until no motion is

detectable, resulting in mechanical spinal fusion. “Open technique” spinal fusions are long and taxing surgeries, exposing patients to complications and challenging post-operative convalescence [1,2]. To minimize surgical morbidity, minimally invasive (MI) spinal fusion techniques have developed, with their promise for less surgical trauma, shorter hospital stays, quicker recoveries and fewer peri- and post-operative complications [3,4]. Taken to an extreme, MI spine fusion could be an injection-based percutaneous treatment that induces heterotopic ossification sufficient to mechanically stabilize the intended spinal segment(s), possibly eliminating surgery, recovery, and major complications all together. Percutaneous or relative-MI delivery of a variety of treatments in comparative models to induce posterior [5,6] and anterior [7–10] fusions offer hope that percutaneous fusion may be possible for clinical use one day.

We previously delivered bone morphogenetic proteins (BMPs) to endplate-punctured but otherwise intact lumbar intervertebral discs (IVDs) in Lewis rats, and observed that, although we could induce bone anterior to the IVD, the nucleus pulposus (NP) compartment of the IVD was well preserved and was remarkably resistant to osteogenesis [7]. We used non-invasive induced angular displacement (NIAD) at 4-week intervals to measure the loss of spinal motion over time, and showed the pre-operative NIAD measurement decreased in all surgical groups (attributed to soft tissue scarring) by ~25%, but only the heterodimer BMP group showed progressive NIAD losses beyond 4 weeks. BMP-induced bone formation was dose-responsive to the relative osteoinductiveness of the treatment delivered (heterodimer (BMP2/BMP7) > homodimers (BMP2 or BMP7 or mixed BMP2 + BMP7) > negative control (betagalactosidase)), but significant spinal fusion was only observed for the heterodimer-treated group. Progressive loss of NIAD over the course of the experiment predicted relative bone production, increased stiffness assessed by 4-point bend biomechanics, and spinal fusion (assessed by palpation and radiographic endpoints). Our findings supported the opinion that the NP is a very inhospitable location to induce bone formation, either due to the known IVD avascularity and hypoxia, or other non-vascularity-related mechanisms that make the NP a barrier to neo-osteogenesis.

Considering the disc as a physical or chemical barrier to bone induction, we hypothesized that a treatment to remove the IVD matrix could render the disc better able to support bone induction for fusion. Chymopapain is perhaps the most familiar of the enzymes used experimentally and clinically as a chemonucleolytic agent (a substance able to dissolve disc tissue) [11,12]. A second-generation agent, chondroitinase ABC (chABC), is safer than chymopapain in comparative models including hamsters, rabbits and pigs [13–16]. Previously, application of chABC to (Sprague Dawley) rat IVDs decreased proteoglycan content and altered spine and IVD mechanics [17,18]. Due to the safety profile, demonstrated experimental utility, and commercial availability, chABC was selected to chemically degrade the IVD in our rat anterior spine fusion model.

How avascularity is normally maintained in the NP, and therefore how it might be manipulated, is poorly understood despite the multiple molecules and mechanisms that have been suggested, including tissue inhibitor of metalloproteinase-3 (TIMP3) [19], semaphorin 3A [20], thrombospondin-1 (TSP1) [21], TSP2 [21], TSP3 [21] and TSP5/collagen oligomatrix protein (COMP) [22], or chondromodulin-1 (CHM1) [23] and the related molecule tenomodulin (TNMD) [24]. Furthermore, when the expression of these molecules was manipulated and IVD angiogenesis assessed, angiogenic vessel penetration in the annulus fibrosus (AF) was observed, but the NP remained avascular [20,25–27], suggesting *unique* or *redundant* mechanisms for angiogenesis control for different parts of the IVD (NP, AF and cartilage endplate (CEP)) [27,28]. To make the angiogenesis mechanism even more complex are the more recent findings that resident NP cells express vascular endothelial growth factor-A (hereafter, VEGF) [29–33], with VEGF expression being upregulated by IVD hypoxia [31,34,35] and degeneration [29,30,35], downstream of hypoxia-inducible factors (HIF)-1 [36–38] and -2 [34], and NP-expressed VEGF appears to act in a paracrine/autocrine manner as a survival factor for NP cells [31,36–38]. Therefore, a thorough description of IVD anti-angiogenesis would need to explain how the AF, CEP and NP repel vascular ingrowth

and how the NP-expressed VEGF is sequestered from acting on angiogenesis-sensitive tissues external to the disc space. We hypothesized that generating a blood supply into the disc would allow BMP-driven bone formation within the IVD, and that angiogenesis inside the IVD could be achieved through VEGF gene delivery into the NP that would overpower the anti-angiogenesis mechanisms.

Osteoinductive signaling through BMP is up-regulated in response to VEGF treatment [39], and reciprocally, VEGF signaling is up-regulated by BMP treatment [40], with both acting as chemotaxis signals for osteoblasts and endothelial cells [41]. Co-treatment with VEGF and BMP produces bone significantly earlier and to a greater extent than BMP alone, and VEGF inhibition impairs BMP-induced osteogenesis [42,43]. Interestingly the ratio of VEGF-to-BMP delivered affected bone induction, with optimal osteogenesis observed with VEGF-to-BMP at a 1:5 ratio [42,43]. This introduces our third hypothesis: co-delivering BMPs and VEGF would augment osteogenesis and fusion in our model.

Here, we hypothesize that (1) intra-discal delivery of cells genetically modified to express VEGF₁₆₅ will overpower the anti-angiogenesis homeostasis mechanisms of the IVD and drive angiogenesis within the IVDs prepared by endplate perforation, making the IVDs permissive for bone induction by BMP, (2) co-delivery of BMP-expressing cells with VEGF-expressing cells will additively or synergistically enhance bone induction and spinal fusion, and (3) chondroitinase ABC delivery will destroy IVD chondroitin/dermatan sulfate aminosaccharide proteoglycans, disrupting the NP inhibition of neo-osteogenesis, and make the IVD permissive to BMP-induced bone formation and spinal fusion.

2. Materials and Methods

2.1. Preparing Treatments and Animal Surgeries

Bone marrow mesenchymal stromal cell (BMSC) cultures, virus stocks, and transgene-expressing BMSCs for implantation were generated as previously described [7,44,45]. All animal surgeries and primary cell cultures were performed under a Hospital for Special Surgery (HSS) Institutional Animal Care and Use Committee (IACUC) approved protocol (#03-08-06R), and in compliance with ARRIVE guidelines and HSS Center for Lab Animals Services (CLAS) guidelines and regulations. BMSCs from $n = 20$ male approximately 8-week-old (200–250 g) Lewis rats were expanded in monolayers, transduced 18–24 h prior to surgery with 10^5 particle units (pu)/cell with recombinant adenoviral (Ad) vectors encoding human bone morphogenetic protein-2 (AdBMP-2), human BMP-7 (AdBMP-7) and human VEGF₁₆₅ (AdVEGF) transgenes, and a sample of the gene-programmed cells was assessed 3 days after transduction for transgene expression using ELISA (VEGF and BMP2 using kits from R&D Systems Inc., Minneapolis, MN, and BMP7 using a kit from Alpha Diagnostic International, San Antonio, TX, USA). When representative aliquots of cells demonstrated lack of intended gene expression, implanted animals were immediately euthanized ($n = 59$).

Experimental groups were designed to receive equivalent treatment dosages to allow direct comparisons between groups. Just prior to implantation, cells were trypsinized, concentrated by centrifugation, counted by hemocytometer, and suspended in growth media into a slurry so that 10^6 cells would be delivered in 25 μ L, a previously optimized dosage [44]. Chondroitinase-ABC (chABC, Sigma, Burlington, MA, USA cat# C2905) was used at a dose of 25–30 milli-Units. A non-operated group (Mock) and an operated group implanted with non-Ad-infected cells (Naïve) were included as negative controls. Operated treatment groups were chABC (implanted with chABC and 6 parts naïve cells), VEGF (implanted with 1 part AdVEGF-infected cells and 5 parts naïve cells), BMP (implanted with 1 part naïve cells and 5 parts AdBMP2 and AdBMP7 doubly transduced cells), and all combinations of these three treatments, with the group size ($n \geq 15$ animals) determined by power analysis for the primary outcome of palpation fusion.

Treatments were implanted into the L4–L6 disc spaces. Approximately 8-week-old (200–250 g) male Lewis rats ($n = 221$) were anesthetized, sterilely prepared and subjected to a transperitoneal exposure of lumbar levels L4–L6, as previously described [7,44,45].

Vertebral endplates were punctured using a 22 Ga needle passed through the anterior L5 body proximally into the L4 body (through the L4/5 disc), and repeated directed distally into the L6 body (through the L5/6 disc); 2–3 passages per disc were performed. Using a 25 Ga needle, 10^6 genetically modified BMSCs were delivered to L4/5 and L5/6 disc spaces, and wounds were closed in layers. Animals were recovered, and allowed ad libitum food, water and activity. Morbidity and mortality data have been reported separately [45].

2.2. Noninvasive Induced Angular Displacement Assessments

High-definition digital Faxitron radiograph images were used to monitor spinal non-invasive induced angular displacement (NIAD) throughout the time course as we have described [7,46]. Pre-operatively ($n = 216$) and at 4, 8, and 12 weeks ($n = 136$) after surgery, NIAD quantification was performed under isoflurane anesthesia, with the animals positioned supine in a custom 90-degree bending bracket (in both right and left bending positions), segmental angles were measured for each level L4–S1, and data are reported as the sum of the right and left angles for each level (total coronal plane displacement). A subset of the images was measured by a second blinded investigator to measure inter-observer reliability using the Interclass Correlation Coefficient (ICC). NIAD data were normalized to the time-zero treatment group means to correct for small groupwise differences in the baseline assessments (Figure A1 in Appendix A), and are presented as ‘Percent of Pre-OP’ in the manuscript.

NIAD assessment at 12 weeks was also adapted as a fusion prediction technique, with fusion defined as segmental measurements that were at least 3 standard deviations below the mean values of the preoperative total population ($n = 216$). For the L4/5 level, the average was 21.6° and the standard deviation was 2.6° , making post-operative specimens considered as “fused” when their NIAD measurement was under 13.8° . For L5/6 the average \pm St Dev was $18.9^\circ \pm 3.5^\circ$, with “fused” defined as under 8.4° , and for L4–6, it was $37.7^\circ \pm 4.4^\circ$, with “fused” defined as under 24.5° . These “NIAD fusion” critical values would be expected to identify the lowest 0.15% of “normal” motion in the pre-operative cohort, and none of the pre-operative animals met these criteria for “NIAD fusion”.

2.3. Bone Formation and Fusion Assessments

Euthanasia, post-mortem radiography, and radiographic bone induction/fusion was performed as we have described [7]. Animals were euthanized at 12 weeks by CO₂ inhalation followed by cervical dislocation. AP and lateral Faxitron images were used to evaluate for unintended heterotopic bone production in the thorax and abdomen, but none was noted. The lateral Faxitron images were also used to score bone induced and probability of fusion of the L4/5 and L5/6 levels. *Graded bone formation* and *fusion likelihood* were assessed on lateral radiographs by 3 blinded investigators for each level using a 0–2 scale: 0 assigned to minimal-to-low-level bone production and suspected non-fusion status, 1 assigned to intermediate bone production and possible fusion status, and 2 assigned to a large amount of bone production and highly likely fusion status. Rater grades were summed for each level independently, and interpreted as follows: 0–2 as minimal bone production (not fused), 3–4 moderate bone production (possible fusion), and 5–6 abundant bone production (fused). Sums were used to compare groups for treatment effects, and dichotomous rendered data (5–6 was fused, 0–4 was not fused) were used for comparisons of fusion assessment methods. *Categorical* radiographic fusion (presence/absence of bridging bone on lateral image) was performed by 3 raters independently, with sample status assigned by the majority.

Spines from euthanized animals were recovered, and palpation fusion assessment was performed as previously described [7]. Spines from L3–S1 were explanted and stripped of soft tissues other than near the intervertebral discs and induced fusion bone. Manual palpation has been reported as the “gold standard” for rat spine fusion assessment [47,48], and was considered as the ground truth for sensitivity, specificity and positive/negative predictive values reported. All spines were palpated by 3 blinded observers for fusion

at L4/5 and L5/6, and were graded as “fused” = no motion, or “not fused” = motion detected; score sums from 3 raters were used to statistically test treatment effects, and dichotomous fusion status by level was assigned by majority for reporting fusion success and correlation testing.

2.4. Micro-CT/Histology and Biomechanics Assessments

Spines were prepared for micro-CT and histology or in vitro biomechanical testing as previously described [7]. Samples were either stored frozen (-80°C) for mechanical testing ($n \geq 10$ /group) or were fixed for 48 h with 4% paraformaldehyde in codylate buffer for micro-CT and histological analysis ($n = 5$ or 6 per treatment group). Quantitative micro-CT scans of rat spines from L3–S1 were digitally reconstructed, processed using GE MicroView software (latest version 2.1) (GE Healthcare, Chicago, IL, USA), and quantified with the mineral threshold set at 1500. Measurements obtained were total volume fusion bone induced for the combined L4–6 segment, and bone formed within the L4/5 and L5/6 discs. Following micro-CT, samples were processed for histology with decalcification in EDTA, paraffin embedding, sagittal sectioning at 5 μm , and staining with H&E (general morphology), Alcian Blue (cartilage), Picosirus Red (collagen), and immunostained for VE-cadherin (BV9, Santa Cruz Biotechnology Inc, Dallas, TX) with selected samples undergoing follow up immunostaining with CD31 (ab182981, Abcam PLC, Waltham, MA). Mid-sagittal sections were chosen for scoring, samples were re-sectioned or re-embedded to obtain optimal appearance, and histological assessments of a disc were excluded unless one or both endplates showed a surgical puncture site from the disc preparation (except the Mock group where midsagittal was estimated). The L4/5 and L5/6 levels were assessed and scored independently, making possible specimens per group $n = 10$ –12, but with midsagittal requirement applied, the actual numbers were $n = 11$ (chondroitinase ABC (chABC)/VEGF), $n = 10$ (Mock, Naïve, BMP, chABC/BMP), $n = 9$ (VEGF, BMP/VEGF, chABC/BMP/VEGF), and $n = 6$ (chABC). Histology samples were assessed for IVD damage, induced bone and intra-discal vascularity using a rubric (Table A1) adapted in part from prior studies [49–51]. The final score for damage of a sample (0–8) was the sum of 4 sub-scores (NP damage (0–2), AF damage (0–2), alterations in interfaces (0–2) and Alcian Blue staining (0–2)); scores for bone formation (0–3) and angiogenesis (0–2) did not require summation.

Biomechanics specimens were potted and subjected to four-point bending mechanical testing, in vitro angular displacement (IVAD), and four-point load to failure in extension, all as previously described [7,46]. Proximal (L3 and proximal L4) and distal (distal L6 and S1) ends were potted in acrylic bone cement (COE Tray Plastic, GC America, Chicago, IL, USA) in custom rectangular aluminum fixtures, and four-point bending (outer span 50 mm, inner 22.5 mm) was performed over the combined L4–L6 segment with loads applied at 0.5 N/sec up to a maximum of 4 N (ELF 3200, EnduraTec, Eden Prairie, MN, USA). Specimens were assigned numbers, with numbers randomly chosen for processing, and each specimen was tested in random order for right and left lateral bending, and extension and flexion by rotation of the rectangular blocks. IVAD was measured from a digital photograph of the four-point bending apparatus during maximal loading in the 5th cycle for each direction. Four-point-bending moment-to-failure destructive testing was performed in extension, with failure location (L4/5 or L5/6 disc) and moment-at-failure recorded.

2.5. NP Cell and Disc Organ Preparation

Bovine NP (bNP) cell cultures and rabbit disc organs were prepared as previously described [52]. bNP cells were obtained from three cadaveric bovine tails of young adult animals following approval of the HSS IACUC, and in compliance with ARRIVE guidelines and HSS CLAS guidelines and regulations. Discs were dissected, endplates removed, and NP tissue was mechanically and enzymatically extracted. Cells were washed and seeded at 2.8×10^4 cells/ cm^2 density in complete medium (high-glucose Dulbecco’s Modified Eagle Media (DMEM; Gibco, Grand Island, NY, USA), 10% Fetal Bovine Serum (FBS; Gibco), 1% antibiotic-antimycotic (Gibco) and 10 μM HEPES buffer (Gibco)). bNP cells were incubated

in a humidified atmosphere of 5% CO₂ at 37 °C, in either normoxic (not manipulated, 21%) or hypoxic (2% oxygen controlled by a BioSpherix C-Chamber inserted into the same incubator; BioSpherix, Lacona, NY, USA). Cells were used for experiments at passages 2–10, with careful monitoring of cell morphology changes with light microscopy at media changes (Figure A2). New Zealand White (NZW) rabbit disc organs were isolated from young adult animals, following approvals by the HSS IACUC, and in compliance with ARRIVE guidelines and HSS CLAS guidelines and regulations. Spines were obtained after the animals had been euthanized and discarded by independent investigators performing non-spine-related protocols. L1–S1 spine segments were excised, posterior elements and anterior soft tissues were debrided, and lumbar vertebral–disc complexes were recovered allowing isolation of IVDs and NP tissue, with $n = 4$ IVDs obtained from each of $n = 8$ rabbits.

2.6. Western Blotting Experiments

Western immunoblotting of soluble VEGF-R1 (sFlt) was performed using bNP cell cultures and NZW IVD tissue. bNP cells at near confluence had conditioned media collected one day after feeding, the cell monolayer was washed 3 times with ice cold PBS, and the cells and matrix were collected in lysis buffer (10% glycerol, 1% Triton X-100, 50 mM Tris pH 7.5, 150 mM NaCl, 1 mM EDTA, 10 mM NaF, 2 mM Na₃VO₄, 1 mM 1,10-phenanthroline, 4 mM PMSF, and 1x protease inhibitor cocktail (Roche, Basel, Switzerland)). The lysate was incubated on ice for 15 min, clarified by centrifugation (14,000× *g* for 10 min), supernatants were normalized by protein, and prepared for SDS PAGE using 4x Laemmli buffer (Bio-Rad, Hercules, CA, USA). Paired conditioned media samples were normalized by volume and incubated overnight at 4 °C with Concanavalin A-sepharose 4B beads (GE Healthcare, Piscataway, NJ, USA) to enrich N-linked glycoproteins (including sFlt), beads were pelleted, and samples were prepared for SDS PAGE using 1× Laemmli buffer. SDS PAGE, transfer to nitrocellulose membrane, blocking, probing with anti-VEGF-R1 (V4262, Sigma-Aldrich, Burlington, MA, USA) and image capture with SuperSignal ECL (ThermoFisher, Bohemia, NY, USA) were similar to our prior description [53,54]. NZW IVDs were opened with a scalpel and NP contents from 2 discs were pooled into microtubes, suspended in sterile TBS and stored on ice until digestions were performed. Digestions (500 µL) were performed in duplicate for 1, 2 or 4 h, or overnight, in either 0.5% collagenase type II (Worthington Biochemical Corporation, Lakewood, NJ, USA), or 200 mU/mL chondroitinase ABC (C2905, Sigma-Aldrich, St. Louis, MO, USA), suspended in DMEM with 1× antibiotic/antimycotic at 37 °C and shaking at 225 rpm. Collagenase type II was chosen as a control for matrix digestion due to its use in generating NP cell primary cultures (suggesting NP cell tolerance of its activity while it disintegrates the IVD matrix), its description as a mixed *protease* activity (it digests collagen and other matrix proteins), and to demonstrate the difference between matrix *proteoglycan* destruction (chABC) and matrix *protein* destruction. After digestion, cells and debris were clarified by centrifugation (14,000× *g* for 10 min), supernatants were normalized for protein, and soluble N-linked glycoproteins were concentrated using Concanavalin A-sepharose beads. Beads were then pelleted, prepared for SDS PAGE with 1× Laemmli buffer, size separated on 10% gels, transferred to nitrocellulose, blocked, probed with anti-VEGF-R1 and imaged with SuperSignal ECL.

2.7. Statistical Testing and Analysis

Secondary to non-uniform fusion bone induction and consequent non-gaussian experimental spine fusion in the most successful groups, measurement data (NIAD, multimodal fusion, bimodal bone formation, and fusion stiffness) did not meet normal data distribution assumptions of parametric tests, and data were compared using the non-parametric Independent Samples Kruskal–Wallis test (ISK-W), with Dunn–Bonferroni post hoc pairwise testing using SPSS (v.22, SPSS Inc., Chicago, IL, USA), as per our prior reports [7,46]. NIAD rater reliability was measured using ICC (SPSS), and time effects on NIAD assessment was measured by ISK-W after data were stratified by treatment and

dependent groups defined by time of assessment (0, 4, 8 or 12 weeks). Fusion data were compared through the sum of three raters for palpation (range 0–3) and for categorical radiographic fusion (range 0–3), as was faxitron bone formation data (range 0–6). Inter-rater agreement for dichotomous/categorical data (multimodal fusion assessments) was measured by Fleiss' Kappa (www.statology.org/T1/textgreater{fleiss-kappa-excel (accessed on 15 May 2023)). Agreement was interpreted for ICC as *poor* for <0.5, *moderate* for 0.5 to 0.75, *good* for 0.75 to 0.9, and *excellent* for > 0.9 [55]; Fleiss' Kappa was interpreted as *poor to fair* for <0.4, *moderate* 0.41 to 0.6, *substantial* for 0.61 to 0.8 and *almost perfect* for 0.81 to 1.0 [56]. Data correlation was performed using Pearson's r for continuous data comparisons and with Spearman's ρ when one or both data sets were non-continuous (SPSS). Testing of treatment effects for graded fusion data (rendered to fused/not), and of prior fusion data [7] to current data, were performed using the Fisher exact test (GraphPad Prism 9, GraphPad Software, San Diego, CA, USA). The four-point biomechanics failure in extension locations was compared using the One-sample t -test for Proportion (https://www.medcalc.org/calc/test_one_proportion.php (accessed on 18 May 2023)). Summarized data were reported using boxplots (median as a centralizing line, 25th and 75th percentiles as box limits and whiskers representing maximum and minimum data points), histograms, stacked bar graphs, or violin plots (similar to boxplots but directly illustrates the data distribution for ordinal data), and all graphs were generated using GraphPad Prism 9.

3. Results

3.1. BMP and BMP/VEGF Decreased NIAD over a 12-Week Time Course

Compared to the pre-operative baseline, operated groups at 4 weeks showed NIAD decreases for L4/5 and L5/6 ($p < 0.001$ for each level, Figures A3 and A4) and for the L4–6 combined segment ($p < 0.001$, Figures 1 and A5). The NIAD decrease in the operative groups was thought to reflect non-specific surgical scarring (Naïve, VEGF), exaggerated scarring due to IVD proteoglycan destruction (chondroitinase ABC (chABC), and combinations), or possibly the presence of induced bone (BMP and combinations). The BMP and BMP/VEGF treatment groups were most frequently identified as being significantly decreased for each of the segments. The L6/S1 level showed NIAD increases of 3–30% in operated groups ($p < 0.0001$), but did not show treatment effects between the operated groups (Figure A6). At weeks 8 and 12, the BMP and BMP/VEGF treatment effects for some of the intergroup comparisons in L4/5 and L4–6 were diminished or lost, despite significant differences being found for each segment for both time points overall (each with $p < 0.001$). This result was attributed to gradual progressive NIAD decreases after 4 weeks, such as those shown for L4–6 chABC (Figure 1), and to more data dispersion in the BMP and BMP/VEGF measurements at 8 and 12 weeks (Figures 1 and A5). Comparing operated groups for the L5/6 and L6/S1 levels also showed some gains and losses of significant treatment effects over time, but BMP/VEGF was most frequently identified as the different treatment (Figures A4 and A6). The lack of more significant NIAD attenuation for the chABC/VEGF/BMP and chABC/BMP groups was surprising, as chABC, BMP and VEGF/BMP treatment all caused significant attenuations, but when combined, there was (or trended towards) less NIAD attenuation, as if the combination of chABC with BMP or VEGF/BMP were antagonizing one another (Figures 1 and A3–A6). When stratified by treatment to allow testing of the effect of time, NIAD data (L4/5, L5/6, and L4–6) showed significant differences for each level of each operative treatment ($p \leq 0.001$), with the exception of naïve cell implantation at L5/6 ($p = 0.308$). The most consistent differences were between pre-operative to any post-operative assessment of a treatment, with only chABC treatment demonstrating progressive loss of NIAD after 4 weeks for the L4/5 ($p = 0.045$ to 0.002) and L4/6 ($p = 0.017$ to 0.02) segments (Figure 1). ICC inter-rater reliability for the NIAD data was *good* at 0.884 (95%CI 0.869 to 0.897, $n = 1072$, $p < 0.001$). No differences were noted comparing the current 12-week NIAD results to our prior published findings (Table A2).

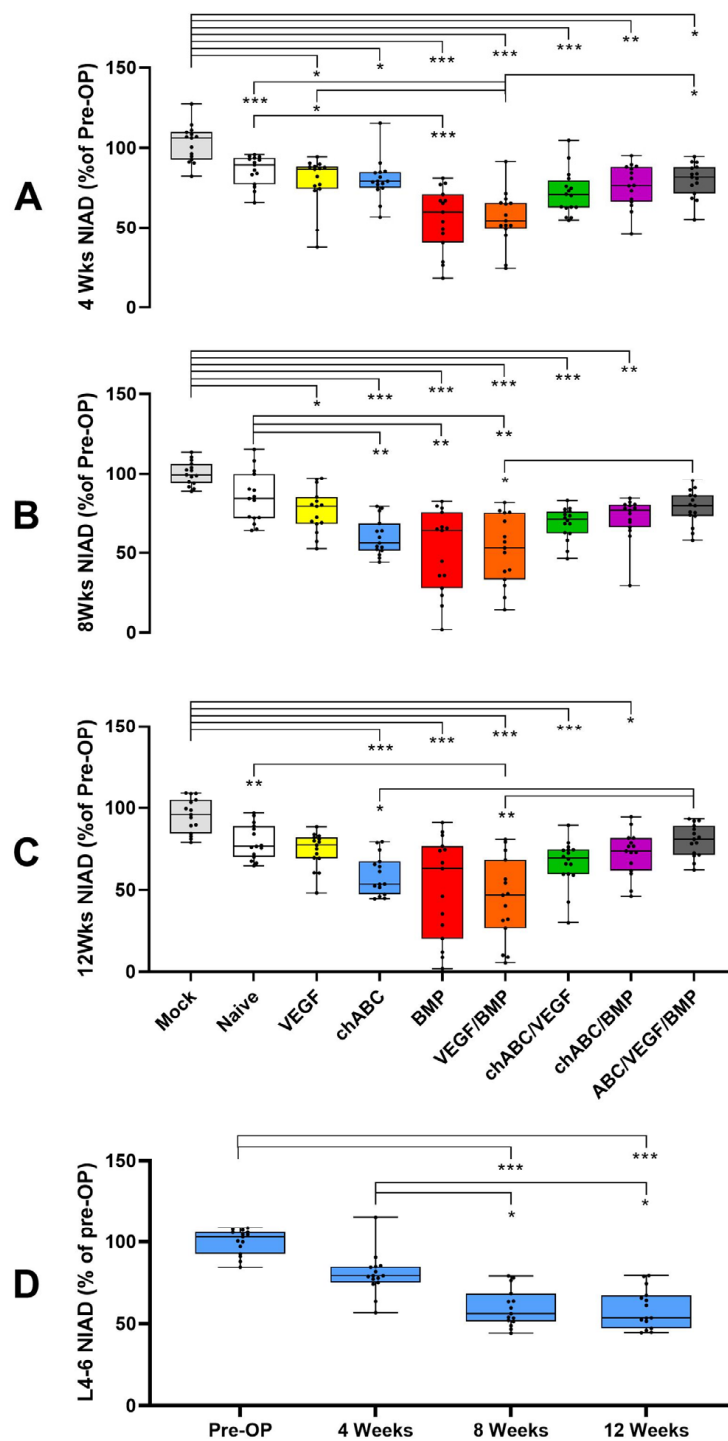


Figure 1. Coronal NIAD assessments for the combined L4–6 motion segment after L4/5 and L5/6 intra-discal delivery of indicated treatments. Panels represent all treatment groups at 4 weeks (A), 8 weeks (B) and 12 weeks (C) post-operatively, or the chondroitinase ABC (chABC) treatment group at 0, 4, 8 and 12 weeks (D). Indicated significance: $p \leq 0.001$ (***), $p < 0.01$ (**), and $p \leq 0.05$ (*).

3.2. Mechanical Stiffness Testing Parallels NIAD Findings and Independently Confirms BMP- and BMP/VEGF-Dependent Increased Spinal Stiffness

IVAD assessment for the combined L4–6 segment showed significant treatment effects between groups in each simple (left, right, flexion and extension) and combined (coronal and sagittal) direction assessed ($p < 0.001$, Figures 2 and A7). Treatment effects were most numerous in the right and coronal comparisons, and the BMP and BMP/VEGF

treatments stiffened the spines more predictably than others. Presumably secondary to inducing soft tissue scarring in or around the IVD, chondroitinase ABC (chABC) treatment caused significant stiffening in the coronal (Figure 2) and left-bending (Figure A7) IVAD directions, but as was found for NIAD, this chABC-induced IVAD stiffness was not augmented by combination with BMP or BMP/VEGF treatments (Figures 2 and A7). BMP- or BMP/VEGF-induced stiffness had a similar antagonistic effect when combined with chABC. Non-destructive four-point bending demonstrated significant differences only in left ($p = 0.003$) and right ($p < 0.001$) bending (Figure 2), but not in flexion ($p = 0.136$) or extension ($p = 0.211$) (Figure A7), and only BMP and BMP/VEGF treatments had significant inter-group differences. Load to failure in extension was affected by treatment ($p = 0.031$), but the only significant intergroup difference detected was between Naïve and chABC treatments ($p = 0.007$). Spine failure location (L4/5 or L5/6 level) was dictated by the fusion status of the level for fused specimens ($n = 14$), was not determinable in some cases ($n = 4$), and these samples ($n = 18$) were excluded from the failure site comparison. Consistent with our prior work [7], spine failure was more likely to occur at L5/6 (52/72) than L4/5 (20/72) ($p < 0.001$, $z = 3.767$, 95%CI: 60.39% to 82.12%), suggesting that L4/5 and L5/6 differ with regard to mechanics or healing potential. The IVAD and NIAD correlated significantly ($r = 0.788$, $p = 0.01$, $n = 90$), consistent with our prior study [7]. No differences were noted comparing our prior results to the current biomechanical stiffness data or to IVAD for samples receiving BMP treatment; however, small but significant differences were found for IVAD-negative controls (Naïve versus Ad-LacZ expressing), potentially due to a subtle effect of the Adenoviral vector and altered data distributions in the datasets (Table A2).

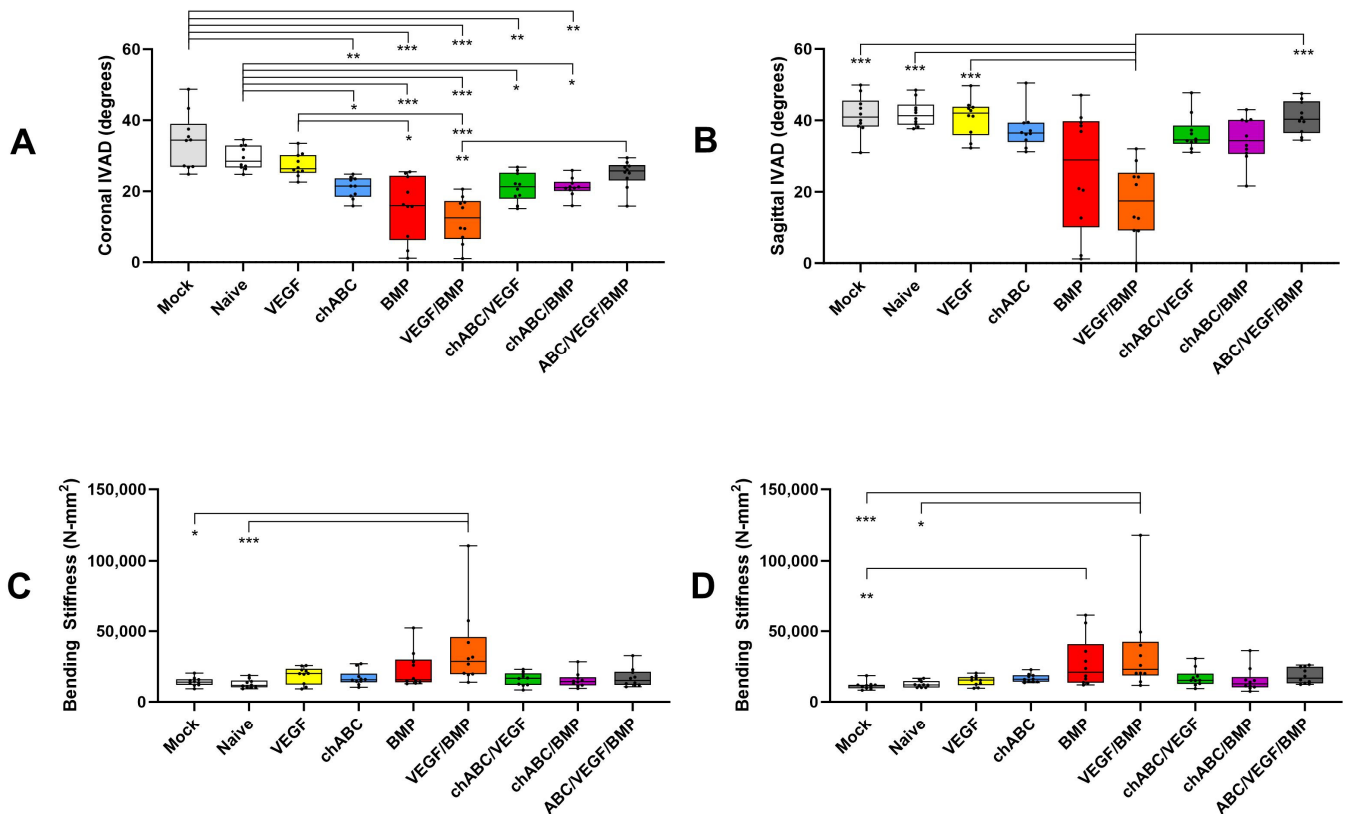


Figure 2. In vitro angular displacement (IVAD) and non-destructive four-point bending mechanical assessments of the combined L4–6 motion segment at 12 weeks post-implantation of the indicated treatments. IVAD is shown in in the coronal (A) and sagittal (B) planes, and four-point bending stiffness is shown in the left (C) and right (D) bending directions. Chondroitinase ABC is abbreviated as chABC. Indicated significance was $p \leq 0.001$ (***), $p < 0.01$ (**), and $p \leq 0.05$ (*).

3.3. BMP and BMP/VEGF Treatment Resulted in Increased Frequency of Spinal Fusion Assessed at 12 Weeks

Manual palpation testing was consistently positive in only in the BMP and BMP/VEGF treatment groups (Figure 3A). BMP and BMP/VEGF fusion rates did not differ by level for each treatment ($p \geq 0.544$) or by treatment at each level ($p = 1$). Although chondroitinase ABC (chABC) treatment did not demonstrate an ability to drive fusions when assessed by palpation (Figure 3A) or by radiographic (Figure 3B,C) assessments, when chABC was combined with BMP or VEGF/BMP, it antagonized the ability of BMP or VEGF/BMP to drive spinal fusions, in the same manner we observed for NIAD and IVAD. Categorical (Figure 3B) and Graded (Figure 3C) radiographic fusion also occurred most frequently in the BMP and BMP/VEGF groups. No differences were noted between the current findings and our prior published results for palpation, or categorical or graded fusions (Table A2). Fusion success measured by 'critical' NIAD values at 12 weeks was similar to the other fusion modalities for BMP and BMP/VEGF (Figure 3D), but additional treatment groups also met this 'NIAD fusion' definition, resulting in a worse positive predictive value (PPV 44.1%) than graded fusion (PPV 92%) and categorical fusion (PPV 84.4%) when palpation success was used as the ground truth. The 'critical' NIAD measurement appeared to be a better assessment of stiffness than actual fusion. Interestingly, 'critical' value NIAD illustrated a trend for treatment interaction, decreasing the stiffness generated by chABC alone when combined with VEGF, BMP or VEGF/BMP, and showing statistically significant antagonism for the L4–6 combined segment comparing BMP or VEGF/BMP \pm chABC (Figure 3D). Agreement between observers was *almost perfect* for palpation (Fleiss' K = 0.869) and categorical fusion (K = 0.818), and was *substantial* for graded fusion (K = 0.709).

3.4. Decreased Mobility and Increased Spinal Fusion Was the Result of Bone Formation around the L4/5 and L5/6 IVDs, but Not Bone Production Inside the IVDs

Bone formation was assessed using high-definition Faxitron radiographs (Figure 4) and micro-CT (Figures 5 and A8). Faxitron assessment showed more moderate/abundant (M/A) bone induction with BMP treatment at L4/5 ($p \leq 0.05$ for treatment comparisons other than chondroitinase ABC (chABC)/BMP ($p = 0.102$) and BMP/VEGF ($p = 1$)) and at L5/6 ($p \leq 0.05$ for treatments other than chABC/BMP ($p = 0.07$) and BMP/VEGF ($p = 1$)) (Figure 4). VEGF/BMP had similar behavior, with more faxitron-assessed M/A bone induction at L4/5 ($p \leq 0.01$) and L5/6 ($p \leq 0.001$) than any other treatment group, other than BMP ($p = 1$). When Faxitron data were not stratified by level, treatment with BMP or VEGF/BMP induced more M/A bone than any of the other treatments ($p \leq 0.001$) with the exception of the BMP to BMP/VEGF comparison ($p = 1$). Micro-CT-based bone assessment similarly favored BMP and BMP/VEGF treatment and bone formation (Figure 5), but significance testing was limited to Mock being different from BMP ($p = 0.004$) and BMP/VEGF ($p = 0.044$). Micro-CT also was used to measure bone formed within the disc space, with Regions of Interest designed to not include endplates or bone external to the disc space, but no significant intra-discal bone was detected for any of the treatment groups ($p \geq 0.528$). We again noted trends for decreased BMP and VEGF/BMP treatment effects (bone production) when combined with chABC. Current data for the combined L4–6 segment demonstrated no differences from our previously published results for faxitron- or micro-CT-based bone formation measurements (Table A2), and induced bone was located anterior to the spine and discs (Figure A8) consistent with our prior findings.

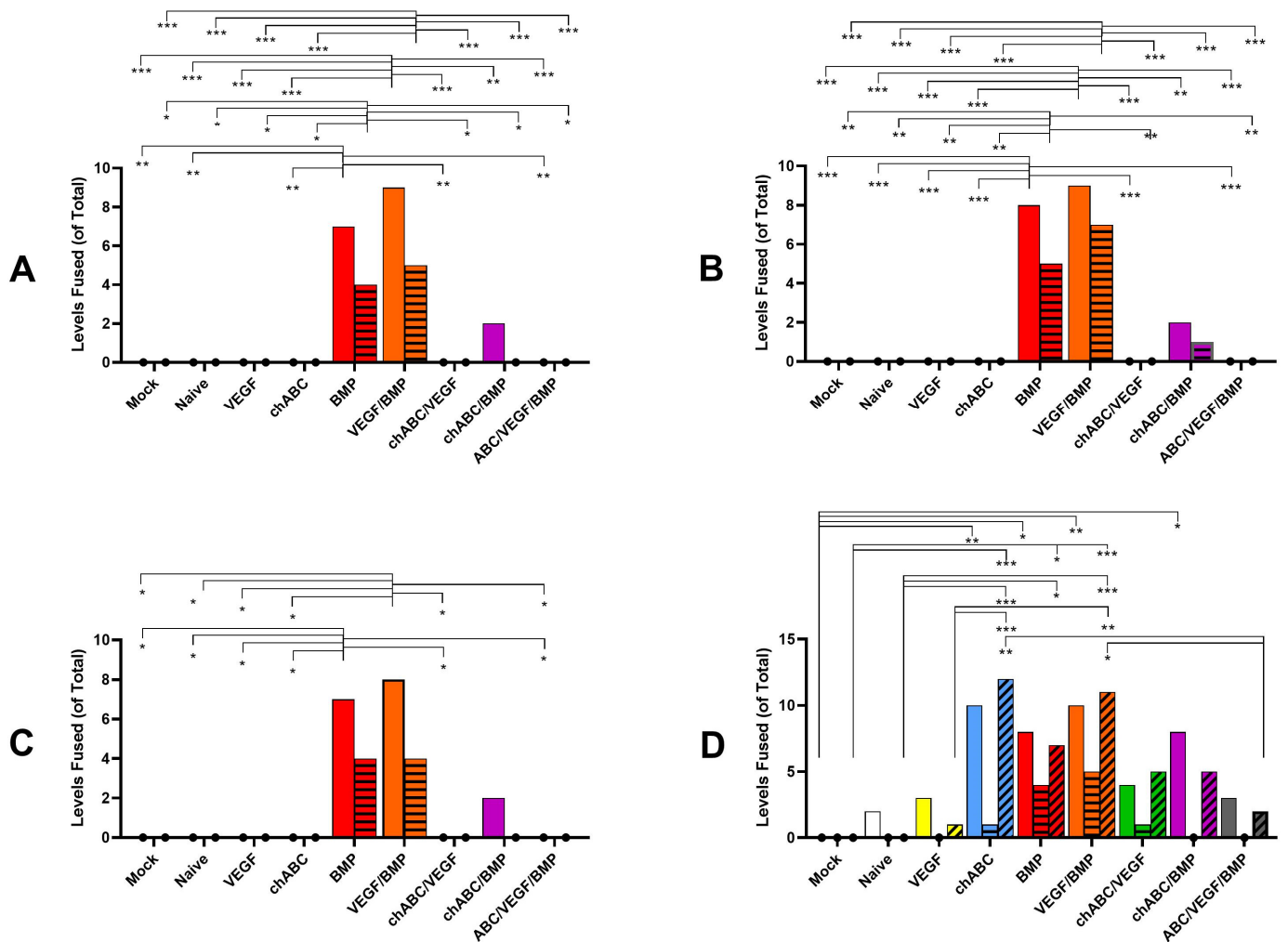


Figure 3. Multimodal spinal fusion assessments at 12 weeks post-implantation of the indicated treatments. Fusion status was scored separately at the L4/5 (histograms with no lines) and L5/6 (histograms with horizontal lines) levels for all assessments, and for the combined L4–6 (histograms with diagonal lines) segment for the NIAD fusion prediction method. Fusion was assessed by palpation (A), categorical radiographic (B), graded radiographic (C), and critical NIAD values (D), as described in the Materials and Methods section. Histogram vertical heights indicate raw value for number of fusions, and group size was $n = 15$ for all treatments except chondroitinase ABC (chABC)/VEGF ($n = 16$). Indicated significance was $p \leq 0.001$ (***), $p < 0.01$ (**), and $p \leq 0.05$ (*).

3.5. Bone Induction Required BMP Treatment, VEGF Treatment Alone Did Not Induce Angiogenesis, and Chondroitinase ABC Did More Damage Than Expected

Light microscopy outcomes focused on assessing damage induced in the IVD, bone induction internal or external to the disc, and induced angiogenesis (particularly in NP tissue) through use of scoring criteria (Table A1). Composite IVD damage was noted in surgical groups in comparison to Mock ($p < 0.05$ for all but Naïve ($p = 0.314$) and chondroitinase ABC (chABC)/BMP ($p = 0.082$)), and the highest average IVD damage was observed in the chABC and chABC/VEGF treatment groups (Figure 6) but inter-treatment comparisons did not reach statistical significance. Less IVD damage was noted when chABC samples were co-treated with BMP ($p = 0.036$) and when chABC samples were treated with BMP instead of VEGF ($p = 0.041$) (Figures 6 and 7). IVD damage included variable loss of Alcian Blue proteoglycan staining in the NP of chABC compared to Mock, Naïve, VEGF and VEGF/BMP (all $p < 0.05$) and of chABC/VEGF compared to Mock and Naïve (both $p < 0.034$). Operated samples compared to Mock all showed loss of biphasic NP staining ($p < 0.001$), and variable production of collagen stranding in the NP space (demonstrated

by positive picosirus red staining visualized with circular polarized light) that did not demonstrate a treatment effect in post hoc testing. AF waviness and clefts were present more frequently in chABC-treated samples than Mock ($p = 0.044$), and in chABC/VEGF-treated samples than Mock, Naïve, VEGF, BMP and chABC/BMP treatments ($p < 0.05$ for each). Bone induction was most pronounced in the BMP and BMP/VEGF groups ($p \leq 0.001$ when either was compared with Mock, Naïve, VEGF, chABC and chABC/VEGF), and was also induced in less abundance in the chABC/BMP ($p < 0.02$ compared with Mock, Naïve, VEGF, and chABC/VEGF) and chABC/BMP/VEGF treatment groups ($p < 0.05$ compared with Mock, Naïve, and chABC/VEGF) (Figures 6 and 7), again suggesting antagonism between chABC and the BMP and BMP/VEGF groups, but no significant differences were noted between BMP or BMP/VEGF \pm chABC post hoc comparisons. Unexpectedly, angiogenesis into the NP was not significantly detectable in the VEGF monotreatment group, but was observed in the chABC ($p < 0.02$ compared with Mock, Naïve and chABC/BMP treatments) and chABC/VEGF groups ($p < 0.05$ compared with Mock, and $p = 0.283$ when compared with Naïve or chABC/BMP) (Figures 6 and 7). Angiogenesis was frequently associated with a fibrocartilage AF-like discordant healing response where the NP is usually located (cranial-caudal AF-like organized bundles that stain intensely with Picosirus Red) (Figure 7, see chondroitinase ABC/VEGF). This pattern was most commonly observed in the chABC and chABC/VEGF groups.

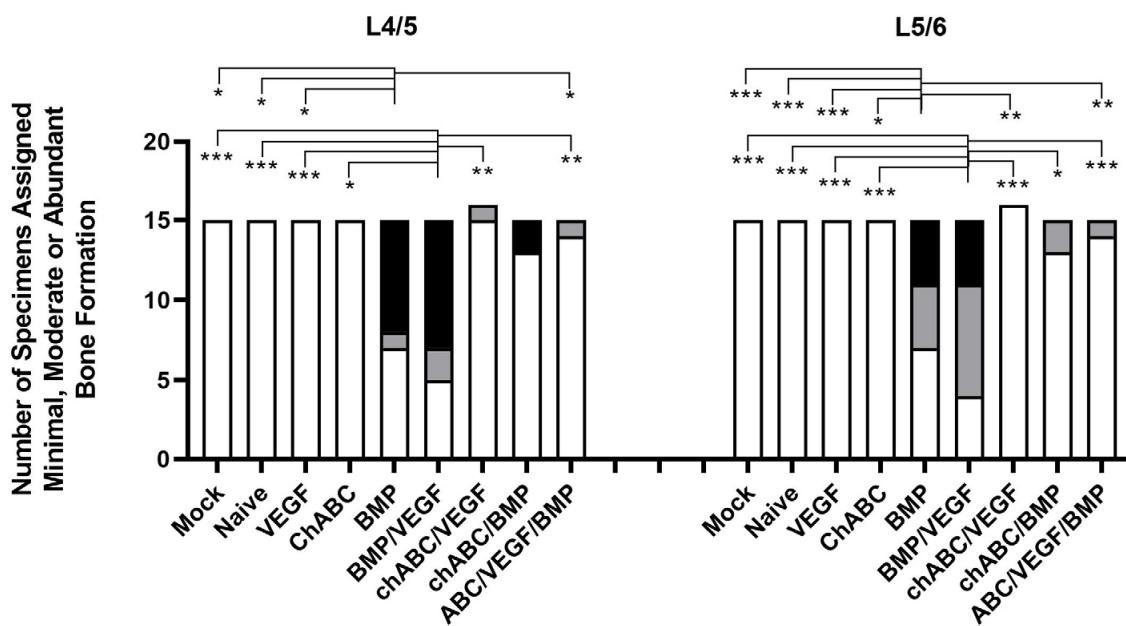


Figure 4. BMP-driven bone induction as assessed by high-definition Faxitron radiographs. Groups are composed of $n = 15$ or 16 specimens, the L4/5 and L5/6 levels were scored independently, and scoring and data testing were conducted as described in M&M. Histogram filled with white background indicates Minimal bone formation, gray indicates Moderate bone formation, and black Abundant bone formation. Chondroitinase ABC is abbreviated as chABC. Indicated significance was $p \leq 0.001$ (***), $p < 0.01$ (**), and $p \leq 0.05$ (*).

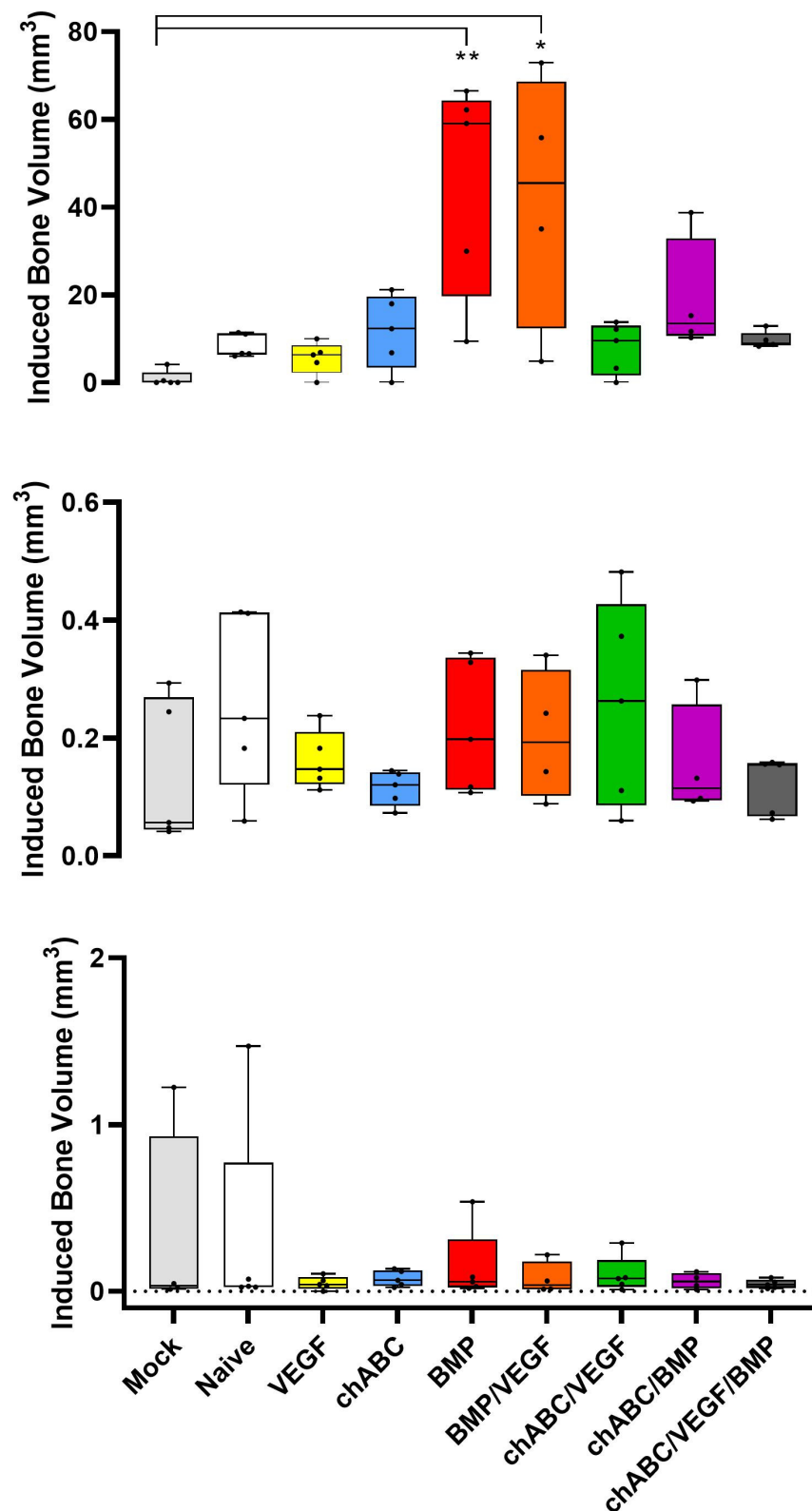


Figure 5. BMP-driven bone induction as assessed by micro-CT. Groups are composed of $n = 4$ (BMP/VEGF and chondroitinase ABC (chABC)/BMP) or $n = 5$ (all other groups) specimens. Specimens were prepared, assessed, and data tested as described in M&M. Top panel shows quantification of induced bone for the entire L4–6 fusion mass (located anterior to the spine and discs), the middle panel shows bone formation inside the L4/5 disc, and the bottom panel shows bone formation inside the L5/6 disc. Indicated significance was $p < 0.01$ (**), and $p \leq 0.05$ (*).

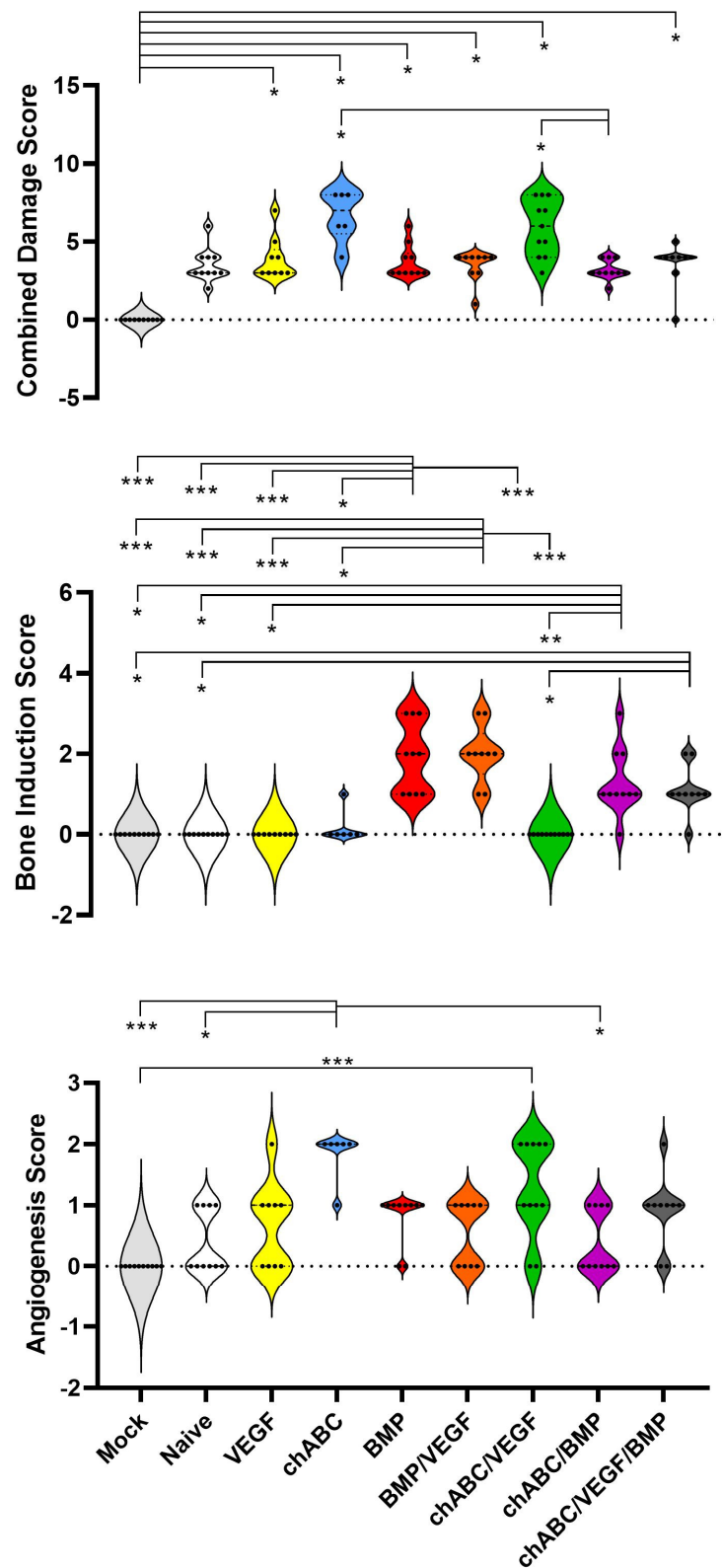


Figure 6. Disc histology scoring results at 12 weeks after intradiscal delivery of treatments. Using a scoring rubric (Table A1), specimens were assessed for IVD damage criteria (top panel, range 0 to 8), osteogenesis extent (middle panel, range 0 to 3) and evidence of angiogenesis (bottom panel, range 0 to 2), as described in the Materials and Methods section. Results are presented using violin plots to demonstrate the distribution of the ordinal data. Chondroitinase ABC is abbreviated as chABC. Indicated significance was $p \leq 0.001$ (***), $p < 0.01$ (**), and $p \leq 0.05$ (*).

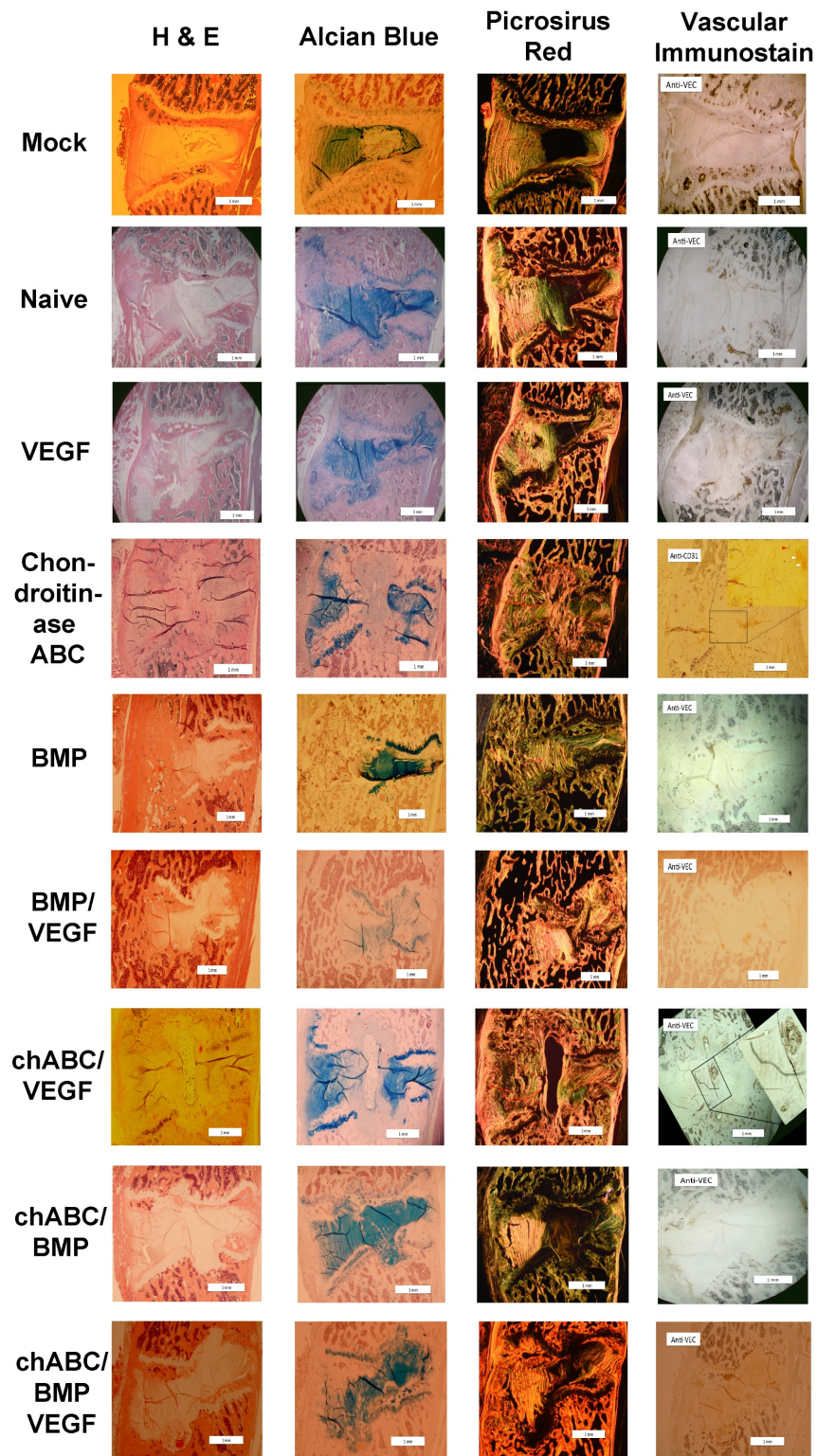


Figure 7. Representative histology images at 12 weeks after intradiscal delivery of treatments. All images are oriented ventral to the left and cranial as top. Histological staining technique is indicated at the top of each column and treatment group is indicated on the far left of each row. Picrosirius Red birefringence was visualized with circular polarized light, and vascular immunostain shown in the figure is anti-VE-cadherin or anti-CD31 (+), as indicated in each panel in that column (upper-left corner). Arrowheads in immunostained images indicate vascular appearing (red arrowhead) or cell clusters (white arrowheads) with positive immunostain. Scale bars in the right lower corner indicate 1 mm. Chondroitinase ABC is abbreviated as chABC.

3.6. Chondroitinase ABC Disrupts Endogenously Expressed VEGF Sequestration, Making the IVD Permissive to Vascular Invasion

We queried the mechanism of Chondroitinase ABC (chABC)-related angiogenesis in our model, and identified a potential role for matrix-bound sFlt. First, we confirmed that chABC causes extensive damage to the NP matrix in our model, including the loss of Alcian Blue staining indicative of decreased proteoglycan content in the NP. Then, recalling that NP cells express VEGF in situ and that the IVD maintains its avascularity despite this VEGF expression must mean that the NP's VEGF is being sequestered and prevented from diffusing through and external to the disc to recruit vascular ingrowth. We suggest that chABC-mediated matrix proteoglycan damage impairs the sequestration capacity of the NP, releasing the endogenous VEGF to diffuse and induce neo-angiogenesis, suggesting a role for proteoglycans or proteoglycan-associated factors in the sequestration process (Figure 8A). Once sequestration is lost, VEGF-activated vascular tissues respond by invading the IVD and following the new VEGF gradient into the NP compartment where the VEGF was being generated (Figure 8B). In such a model, experimental delivery of VEGF-expressing cells to the NP would potentially have no effect on angiogenesis provided that the sequestration mechanism was sufficiently strong, but co-delivery of chABC and VEGF would be expected to possibly result in an even stronger VEGF diffusion gradient, and stronger angiogenesis responses. This argument then begs the question: what is the mechanism that the IVD uses to sequester the endogenously expressed (or experimentally delivered) VEGF? VEGF sequestration molecules could be expressed throughout the disc, or perhaps only in the NP compartment. Our findings would suggest that candidate sequestration molecules would need to be expressed in at least one of the areas where we observed significant matrix destruction: the NP, CEP and growth plate.

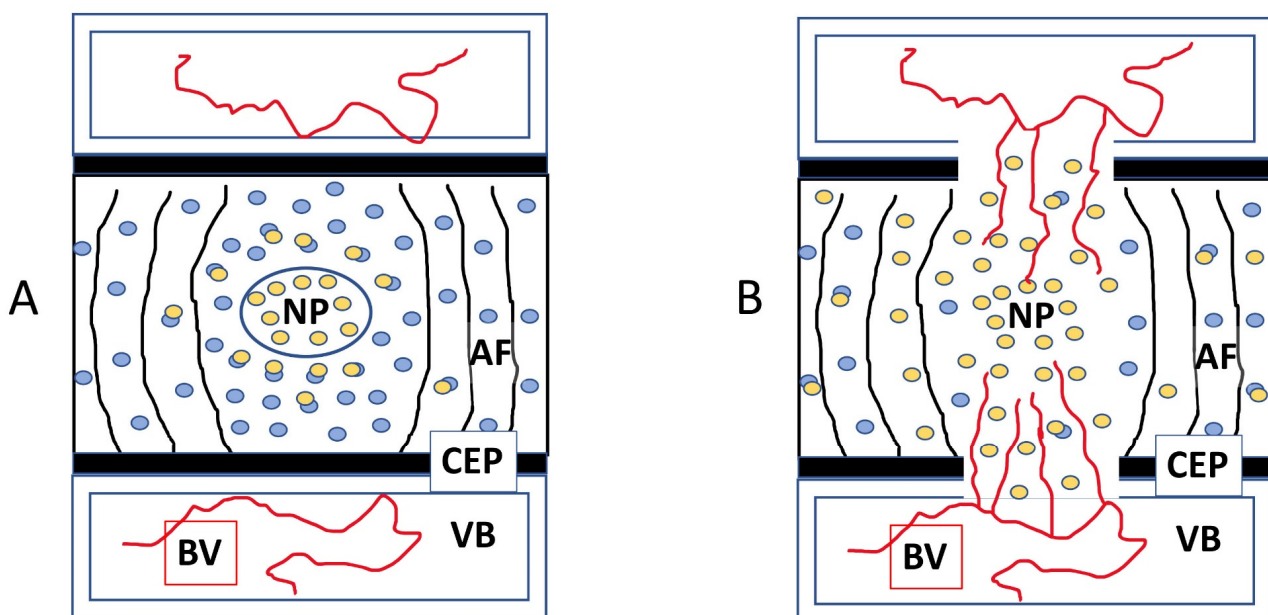


Figure 8. A model for sFlt deregulation in the NP and how it would lead to vascular invasion of the IVD/NP. Major involved structures are labeled with initials: NP = nucleus pulposus, AF = annulus fibrosus, CEP = cartilage endplate, VB = vertebral body, and BV = blood vessels in proximity. Prior to endplate injury and sFlt deregulation, VEGF (yellow ovals) is being bound and sequestered from detection by tissues external to the disc space by sFlt (blue ovals) as shown (A). After sFlt is deregulated, there is reduced sFlt presence in the NP, VEGF is able to diffuse further in all directions, and particularly towards the endplate perforations where VEGF-sensitive blood vessels are positioned and are able to contribute to angiogenesis into the IVD as shown (B).

We used two in vitro models to characterize IVD sFlt, a soluble fragment of the VEGF receptor-1 which could bind and sequester VEGF in the IVD matrix. In tissue cultured NP cells from bovine caudal discs (bNPs) we detected sFlt in the cell/matrix portion of the tissue culture samples but not the media (Figure 9). In freshly enucleated rabbit NP tissue from lumbar spines, we observed that treatment with chondroitinase ABC (chABC - causing matrix proteoglycan destruction), but not collagenase type II (matrix protein destruction), solubilizes sFlt from the cell/matrix of fresh rabbit NP tissue (Figure 9). If sFlt functions to sequester VEGF in the NP in vivo, then the chABC-mediated release of sFlt from the NP proteoglycan matrix could mediate the loss of VEGF sequestration and consequent IVD vascularization that we observed. We are continuing to characterize the role that sFlt or other fractional forms of VEGFR1 (sFlt1-14, or possible shed forms generated by ADAMTS enzymes) serve as regulators of NP anti-angiogenesis.

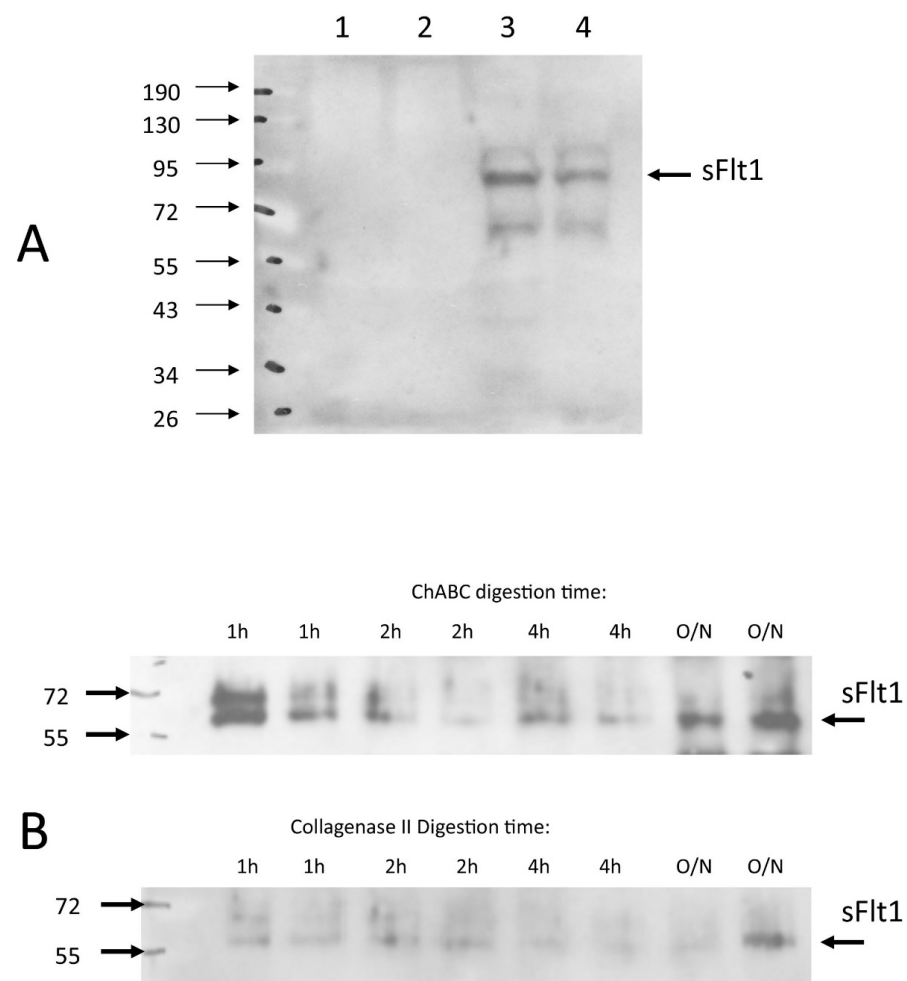


Figure 9. sFlt Western Blotting of bovine NP cells and rabbit NP tissue. Western immunoblotting for soluble VEGF-R1 (sFlt) demonstrated that sFlt was not detectable in supernatant media in bovine NP monolayers ((A), lanes 1 and 2), but rather was found in the cell/matrix fraction ((A), lanes 3 and 4) and this was not altered by normoxia (21% oxygen culture conditions, lanes 1 and 3) or hypoxia status (2% oxygen culture conditions, lanes 2 and 4). Freshly enucleated rabbit NP tissue when subjected to chondroitinase ABC (ChABC in the figure) digestion over time course (see Materials and Methods) released sFlt from the cell/matrix fraction ((B), upper blot), but digestion of sister samples with Collagenase Type II did not consistently solubilize sFlt ((B), lower blot).

4. Discussion

This study has revealed the IVD to be manipulable for angiogenesis, a critical step forward in our evolving rat model to engineer percutaneous IVD fusions for clinical ap-

plication. We showed that IVD delivery of purified chondroitinase ABC (chABC) resulted in the dramatic disorganization/destruction of the NP compartment, loss of proteoglycan staining in the NP and AF, and angiogenesis but not osteogenesis within the IVD. Adding chABC treatment to delivery of BMP-expressing cells did not result in the predicted bone formation inside the IVD, and the combination resulted in almost no bone formation outside the IVD when compared to BMP-expressing cells alone; however, this chABC/BMP combination also resulted in less chABC-induced IVD damage than chABC alone, suggesting an antagonism between BMP and chABC effects. Codelivery of VEGF and BMP also did not result in bone production inside the IVD, and did not significantly increase the amount of bone induced external to the IVD as compared to BMP alone. Gene delivery of VEGF alone was not sufficient to induce angiogenesis in the IVD, and this surprising result may explain, in part, why the addition of VEGF did not promote bone formation in the IVD in BMP-treated spines, because at a first approximation the absence of VEGF-induced IVD angiogenesis makes the VEGF/BMP condition inside the IVD work like BMP alone. Triple treatment with chABC/BMP/VEGF was most similar to VEGF or chABC/VEGF, with some damage and angiogenesis observed but no IVD bone formation, either showing another example of chABC-BMP antagonism or suggesting that factors other than the absence of vascularization inhibit bone formation within the IVD. Finally, we confirmed that the BMP gene delivery technique is reproducible for increasing spinal stiffness, induced bone formation and segmental fusion when the current data were compared with our prior findings from identically treated animals.

A recent Scoping Review examined the English language literature for human disc vascularization, and found no evidence for NP vascularity throughout life, while CEP and AF have early vascularity that involutes at maturity and returns again during degeneration and aging [27]. The non-degenerate NP at maturity is dependent on diffusion for delivery of nutrients and removal of waste [57], is considered to be the largest avascular organ [27,57], and expresses the hypoxia-inducible factors that would be required to up-regulate angiogenesis signaling molecules capable of inducing vascular invasion into the disc space [57,58]. However, despite multiple reports showing that NP cells express VEGF [29–32], the NP remains avascular, as if the NP-expressed VEGF was being sequestered and “hidden” within the IVD to avoid being detected and acted upon by VEGF-sensitive vascular progenitors that could drive angiogenesis. The avascular cornea uses such a system, where the VEGF-expressing corneal cells co-express sFlt (a soluble form of the VEGF receptor-1) that functions to sequester VEGF from the blood vessels of the sclera, and when corneal sFlt expression is experimentally attenuated, VEGF becomes detectable and aggressive angiogenesis onto the cornea is induced [59]. The IVD has been reported to express sFlt [31,60], and this sequestration mechanism for IVD anti-angiogenesis has been suggested, but has not previously been demonstrated [60]. IVD avascularity is very well preserved in vertebrates [31,61], suggesting that a robust set of anti-angiogenesis mechanisms maintains homeostasis, as is also the case for the cornea (including thrombospondin-1 (TSP1) [62], TSP2 [63], TSP3 [64], tissue inhibitor of metalloproteinases-3 (TIMP3) [65], TIMP4 [66], among others [67,68]). Sequestration/regulation of VEGF by sFlt may be a generalizable mechanism, having also been described for several tissues, including ovary [69], kidney [70], placenta [71], hemogenic/endothelial progenitors [72], and others [73,74].

We observed that delivery of chondroitinase ABC (chABC) to the IVD rendered the disc permissive to vascular invasion, and that chABC co-administered with VEGF gene delivery also drives IVD angiogenesis. We have presented preliminary *in vitro* evidence suggesting that extracellular matrix (ECM)-associated sFlt is deregulated by chABC matrix proteoglycan destruction, likely through the solubilization of sFlt from its attachment to proteoglycans in the ECM, thereby rendering it incapable of sequestering VEGF to maintain IVD avascularity. The sFlt was not solubilized by collagenase type II, suggesting that ECM protein destruction is not sufficient for IVD angiogenesis. NP angiogenesis was not observed in the absence of chABC, regardless of delivery of Naive cells, VEGF-expressing, or VEGF-and-BMP-expressing cells, demonstrating that the endplate perforations and surgical

insult is not sufficient for IVD angiogenesis. During disc degeneration, similar damage to the IVD occurs, including loss of NP ECM, but vessel ingrowth into the NP is not robust [27], suggesting that still other anti-angiogenesis mechanisms are present. The NP is a notochord-derived tissue, and as such expresses multiple patterning genes that would be capable of attracting or repelling specific cell populations to establish and maintain the very specific environment of the NP interior [32,35], including repelling vascular invasion (shown in non-IVD tissues) through WISP-2/CCN5 [75], Semaphorin 3E [76] and 3A/Collapsin-1 [77], Noggin [78,79], Endothelin-2 [80], Chordin [78,79], and notochordal chondroitin sulfate [77]. If there was direct evidence that they provided anti-angiogenesis effects in the IVD, any of these notochordal angiogenesis-controlling molecules would fit our data, if it can be assumed that their effect decreases as the IVD cell population vitality does, and that the NP is basically destroyed following chABC treatment. For example, the semaphorins are a set of morphogens that control both nerve and blood vessel patterning, and have been suggested to be a mechanism maintaining IVD avascularity through endothelial cell repulsion [81,82]. Semaphorin 3A is a diffusible factor that is expressed in the IVD at higher levels in the AF than NP, but during degeneration AF expression drops while NP expression increases [20,81,82]. Semaphorin 3A expression would appear to correlate with what is observed with degeneration and AF vascular invasion, and would appear to correlate with what has been reported about the NP remaining relatively avascular despite degeneration [27], but this candidate needs direct assessment as regards its expression levels and function in the setting of chABC treatment.

We observed a correspondence between NP compartment destruction, induced angiogenesis in that location, and an atypical inner-AF fibrocartilage healing response in the IVD that extended through the disc and into the juxtaposed vertebral bodies. This is similar to the appearance of IVDs where HIF-1alpha [36,38] or SHH [37] knockdown resulted in the loss of notochordal NP cells, causing shrinking and degeneration of the NP compartment, and NP replacement by fibrocartilaginous tissue resembling the inner-AF [36,38]. Angiogenesis and the aberrant fibrocartilage healing response may both be examples of IVD homeostasis disruption, secondary to the loss of notochord-dependent inhibitory signaling in the setting of the destroyed NP, that results in the release of both anti-angiogenesis and anti-proliferation of the inner-AF tissues. Further characterization of this fibrocartilage tissue and its behavior is warranted.

The antagonism between BMP and chondroitinase ABC (chABC) treatments is thought to be driven by their differential effects on matrix proteoglycans. The lack of BMP-driven osteogenesis external to the IVD in chABC-treated spines is likely due to impaired endochondral ossification. We previously noted Alcian blue-stained cells between the anterior longitudinal ligament and anterior fibers of the AF in non-fused samples in which fusion bone was otherwise observed [7], suggesting the surgical trauma produced a progenitor population of cells capable of responding to a sufficiently strong osteoinductive signal (such as BMP-expressing cells) by undergoing endochondral osteogenesis. This BMP-driven process would include the production of an extracellular matrix rich in chondroitin/dermatan sulfate-containing (CS/DS) proteoglycans (aggrecan, versican, decorin, and biglycan), that would eventually undergo conversion to bone [83]. As chABC breaks down CS/DS proteoglycan-rich matrices, impaired endochondral osteogenesis and lack of bone formation may not be surprising [84,85]. Within the IVD, on the other hand, the chondrogenic activity of BMP likely limited the chABC-driven IVD destruction. This finding is consistent with other studies, in which BMP treatment drove IVD PG synthesis sufficient to restore radiographic disc height, biochemical assessments, and T2-weighted MRI hydration signal [86,87]. As to which activity dominates (chABC vs. BMP), timing and duration of action likely play critical roles. Adenoviral vectors with CMV promoters classically have about a week of high transgene expression, and then waning but detectable transgene expression out to 2–4 weeks [25,88–90]; chABC is very temperature-sensitive and has a half-life of about 12 h at physiological temperatures [91], although one-time mega-dosing has been reported to allow effectiveness for as long as 3 weeks [92]. Future work could include

varying the dose of chABC delivered in our model, to decrease its duration of effect and potentially allow it to act towards angiogenesis, but block the anti-osteogenesis effect.

We observed that VEGF did not augment BMP-driven osteogenesis in our model, in contrast to previously published results, which have reported that their combined application increased bone formation, and that the mechanism involves each gene upregulating the other [39,42,43]. One reason for the difference between our observation and the prior reports may be our use of the hyper-osteoinductive BMP2/BMP7 heterodimer form of these BMPs [93,94]. In our model the VEGF-treated specimens may have generated expression of homodimer forms of BMPs, but these homodimer BMPs were not sufficiently osteoinductive to drive bone formation and fusion in the model, as we have previously shown [7]. Alternate possibilities are that negative feedback mechanisms driven by the heterodimer osteoinductive signaling suppressed VEGF-mediated endogenous BMP upregulation, or that optimal VEGF:heterodimer-BMP ratio is not 1:5, as has been shown for homodimer BMPs, or that the study was underpowered to detect the augmentative effect. Regardless of the molecular mechanisms, an interesting observation from our model is that angiogenesis occurring in chondroitinase ABC (chABC)/VEGF cotreated discs was not sufficient to support BMP-mediated osteogenesis in the IVD in the chABC/VEGF/BMP treatment condition. Therefore, the presence of a proteoglycan-rich matrix and lack of blood supply may not be the only factors preventing bone formation in the IVD milieu. Future work to further investigate these possibilities is needed to develop a percutaneous method of intradiscal spinal fusion.

5. Limitations

The current work has several limitations. Our study was designed to use NIAD to assess induced spinal stiffness over the 12 weeks of the experiment, which did not require euthanasia nor did it allow histology or other assessments at intermediate time points. We were not able to track the implanted cells, monitor implanted cell viability, or measure transgene expression levels from implanted cells after implantation. Our chondroitinase ABC (chABC) dose was chosen by a critical assessment of the published literature, but as judged by near-complete loss of BMP-induced bone in the chABC/BMP and chABC/BMP/VEGF codelivery conditions, it may have been too high. Future experiments to optimize chABC are warranted to investigate if a lower chABC dose could help support osteoinduction as originally hypothesized. Similarly, we did not identify the optimal ratio of VEGF:heterodimer-BMP for VEGF/BMP codelivery, and a different ratio may have improved osteogenesis as we expected. We chose the VEGF₁₆₅ subtype by comparing the known properties for how well the isoforms diffused through the matrix, where the largest (VEGF₂₀₆) did not diffuse well and may not be detected external to the IVD, the smallest (VEGF₁₂₁) diffused very well and may not allow a concentration gradient to be established to direct the angiogenesis into the IVD, making the predominant mid-sized subtype (VEGF₁₆₅) our favored choice [95]; future work could experimentally assess these other VEGF subtypes to determine the optimal size for this surgical model. We have suggested that sFlt may play a role in sequestering IVD-expressed VEGF and IVD anti-angiogenesis homeostasis, but further investigation is required to validate this mechanism. Similarly, the potential role (or presence) of H-type capillaries (the principal endothelial cell type associated with bone, identifiable by their high expression of endomucin and CD31) [96] was not assessed, and needs to be evaluated in future use of the model. Lastly, the fibrocartilage proliferation/healing response in the IVD requires further study to characterize and understand what is being observed.

6. Conclusions

The delivery of chondroitinase ABC (chABC) to the IVD in our rodent model made the NP compartment of the disc permissive to angiogenesis, but chABC co-treatment nearly abolished BMP-induced bone formation external to the disc space, abolishing fusion ability in those samples. Further work is necessary to modify the current, or engineer an

equally effective alternate, angiogenesis treatment that enables osteogenesis, or develop an osteogenesis treatment resistant to the effects of chABC. We plan to continue investigating the molecular mechanisms controlling NP anti-angiogenesis, alternate ways to affect the NP extracellular matrix or NP expressome, the use of allogeneic implanted cells, and larger comparative models.

Using intradiscal gene- and/or factor-delivery, we have demonstrated that our method for driving bone formation and spine fusion is reproducible, and that angiogenesis can be induced in the NP compartment of the IVD. These observations are definite steps towards our goal to develop a method to induce percutaneous human anterior spine fusions, a technique that would reduce pain and suffering, and reduce or eliminate hospital stays and lost days at work.

Author Contributions: Conceptualization, M.E.C., B.A.R. and O.B.-A.; methodology, M.C.H.v.d.M. and C.H.; validation, C.H., S.R.D., A.K.K. and M.E.C.; formal analysis, S.G. and M.E.C.; investigation, S.R.D., A.K.K., M.K.K., K.W.M., S.G., H.J.K., M.B.G. and M.E.C.; resources, B.A.R., M.C.H.v.d.M., M.B.G. and C.H.; data curation, S.R.D., A.K.K. and M.E.C.; writing—original draft preparation, M.E.C.; writing—review and editing, S.R.D., A.K.K., M.K.K., K.W.M., S.G., H.J.K., O.B.-A., B.A.R., M.C.H.v.d.M., M.B.G., C.H. and M.E.C.; visualization, M.E.C.; supervision, B.A.R., O.B.-A. and C.H.; project administration, M.E.C.; funding acquisition, M.E.C. and M.C.H.v.d.M. All authors have read and agreed to the published version of the manuscript.

Funding: This research was funded by the North American Spine Society, Young Investigator Award Grant (MEC); Surgeon In Chief Research Grant, Hospital for Special Surgery (MEC); Mary Kellen-French Clinician-Scientist Grant, Hospital for Special Surgery (MEC); NIH core center: Musculoskeletal Repair and Regeneration Core Center NIH P30-AR46121 (MvdM); National Institute of Arthritis and Musculoskeletal and Skin Diseases of the National Institutes of Health Under award number T32-AR078751 (KWM).

Institutional Review Board Statement: All animal surgeries and primary cell cultures were performed under a Hospital for Special Surgery IACUC-approved protocol (# 03-08-06R, approved on 17 September 2008).

Informed Consent Statement: Not applicable.

Data Availability Statement: Data generated or analyzed during this study are available from the corresponding author on reasonable request.

Acknowledgments: We are appreciative of the encouraging guidance and mentorship provided by Carl P. Blobel and Adele L. Boskey.

Conflicts of Interest: The authors declare no conflict of interest influencing the representation or interpretation of the reported research results.

Appendix A

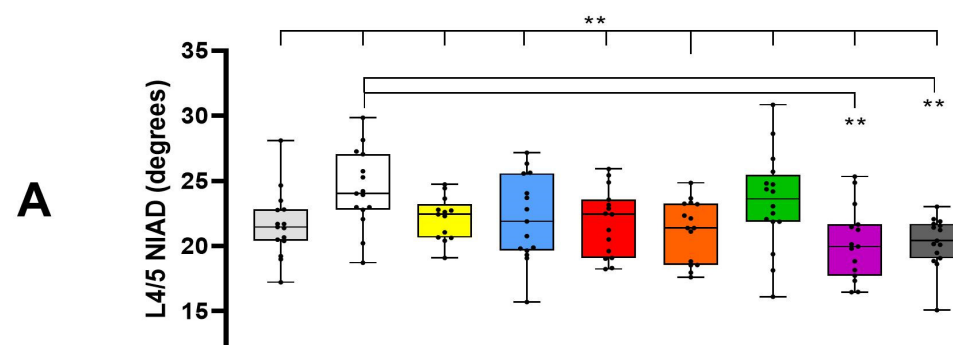


Figure A1. Cont.

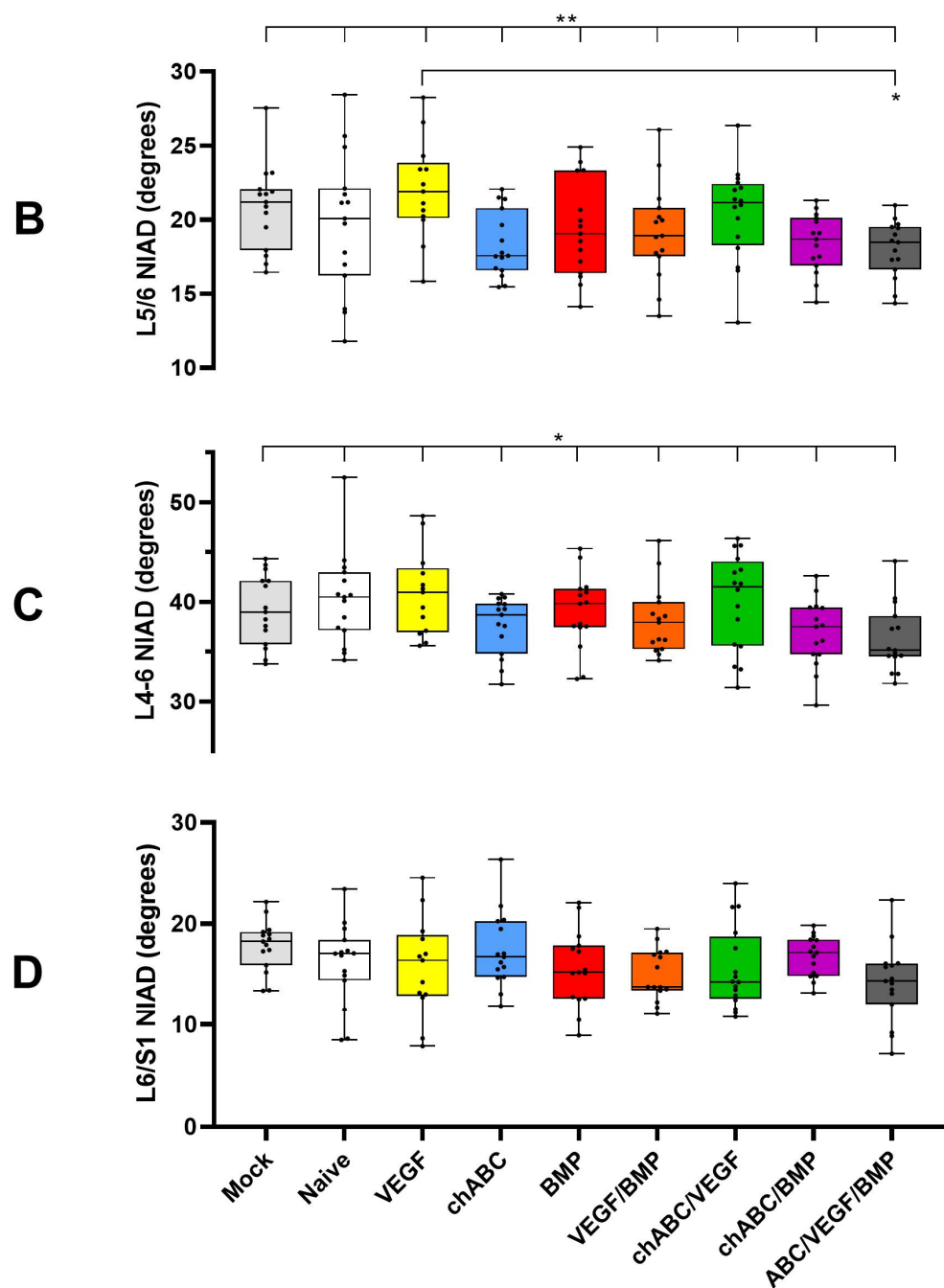
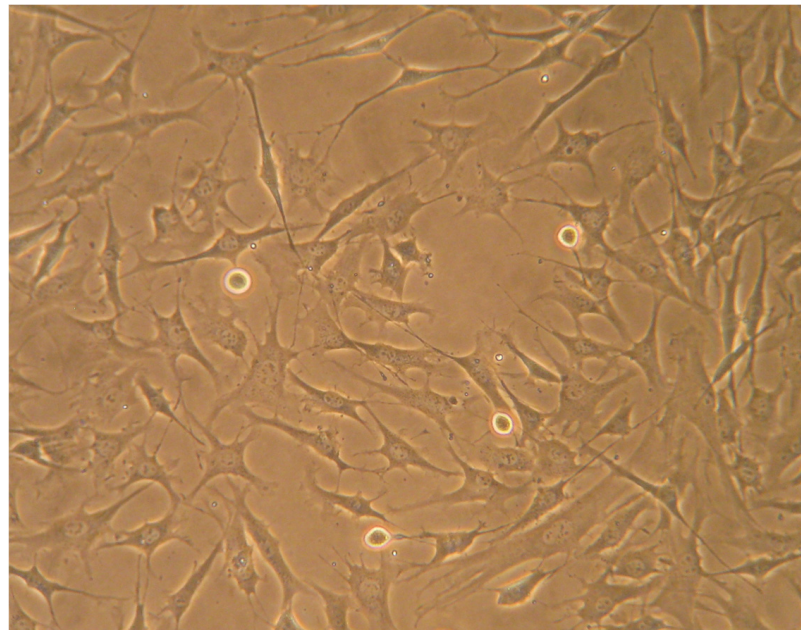
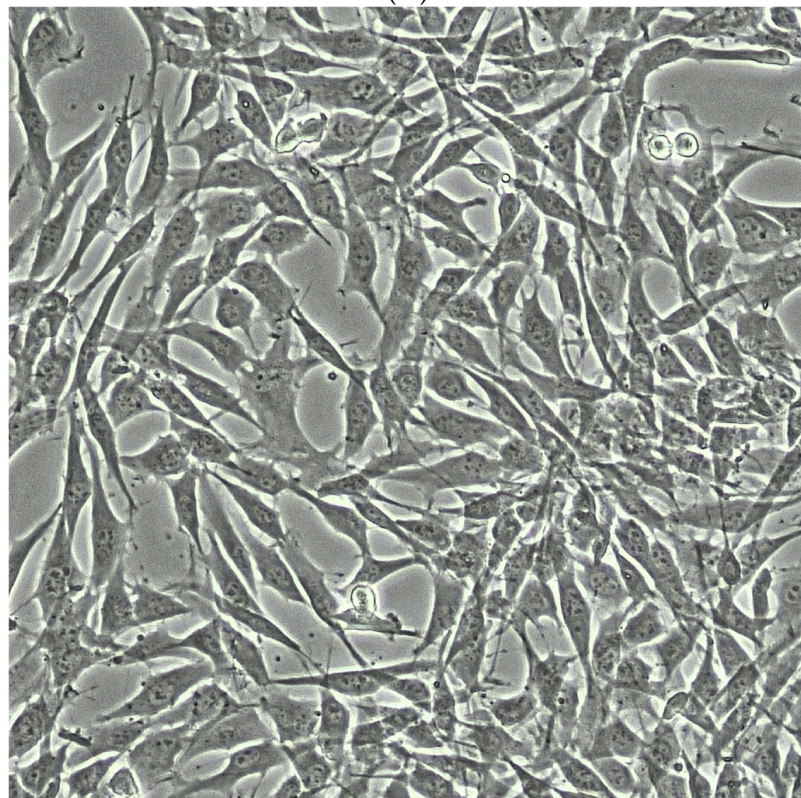


Figure A1. Coronal noninvasive angular displacement (NIAD) assessment of rat lumbar motion segments preformed pre-operatively. Figure panels represent different lumbar levels: (A) L4/5, (B) L5/6, (C) combined L4–6, and (D) L6/S1. Small but statistically significant differences between groups were noted preoperatively, which was addressed by normalizing each specimen to its pre-operative NIAD assessment at the 4, 8 and 12 week NIAD measurements and reporting as ‘% of Pre-Operative NIAD’, as described in Material and Methods. Chondroitinase ABC is abbreviated as chABC. Indicated significance: $p < 0.01$ (**), and $p \leq 0.05$ (*).



(A)



(B)

Figure A2. Bovine nucleus pulposus cultures remain stable after passaging. Primary cultures of bovine nucleus pulposus cells are shown, after harvest from caudal discs as described in Materials and Methods. High-power inverted microscope images are shown, panel (A) are cells at 60–70% confluence being grown up immediately after harvest (passage 0), and panel (B) are passage 10 cells at 80–90% confluence. Both panels show cells being cultured in normoxic conditions.

Table A1. Histology Grading Rubric.

Category	Score	Features	Category	Score	Features
NP Damage	0	Physaliferous cells ⁽⁺⁾ , diffuse/nonfibrotic matrix	Induced Bone Extent	0	No Induced Bone (IB)
	1	PF ⁽⁻⁾ , NP now smaller rounded cells, matrix fibrous stranding (PSR ⁽⁺⁾ staining) not prominent		1	Sparse IB ventral to AF, ± connection to VB (EP-OP/ALL calcification/ossification)
	2	PF ⁽⁻⁾ , small rounded cells, prominent PSR ⁽⁺⁾ matrix		2	Thick IB with organized bone marrow compartment, ventral to AF, but not fused (partially spanning OP)
AF Damage	0	Organized lamellae, no clefts	NP Blood Vessel Structure or Staining Observed	3	IB spanning entire IVD and connecting VBs (IVD fusion)
	1	Wavy/bulging lamellae, mild clefts in outer AF		0	Structures resembling blood vessels ± RBCs, or anti-VEC/anti-CD31 ⁺ immunostaining in only non-induced tissues: VBs, EPs, ALL, PLL, or perivertebral muscle.
	2	Severe lamellae disorganization/bulging, severe clefts		1	Collagen-containing (PSR ⁺) structures resembling blood vessels/RBCs, and or (+) vascular immunostaining cells seen in induced tissues (in VBs or EPs but not into the NP)
IVD Interface Damage	0	Normal NP/EP & AF/NP		2	Blood vessels/vascular immunostain observed crossing into the NP
	1	Loss of NP/EP interface			
	2	Loss of AF/NP interface			
IVD PG Damage	0	Normal Alcian Blue staining			
	1	Reduced AB staining (>50% of control)			
	2	Faint blue to no AB staining (<50% of control)			

Histology definitions for assessment of osteogenesis, angiogenesis and IVD damage present in lumbar discs at 12 weeks following intradiscal injection of naive, or gene-programmed bone marrow stromal cells with or without chABC protein. Lumbar levels L4/5 and L5/6 were considered separately, and scores for osteogenesis, angiogenesis and damage were summed for statistical testing. PF = physaliferous cells in the NP, PSR = picrosirius red staining, AF = annulus fibrosus, NP = nucleus pulposus, EP = endplate, VB = vertebral body, AB = Alcian Blue, PG = proteoglycan, IVD = intervertebral disc, IB = induced bone, OP = osteophyte, ALL = anterior longitudinal ligament, BM = bone marrow, RBCs = red blood cells, VEC = vascular endothelial cadherin, and PLL = posterior longitudinal ligament.

Table A2. Comparison of Current BMP-treatment Outcomes at 12 Weeks to Prior Experiments.

Modality	<i>p</i> -Values for Comparisons					
	L4/5 Segment		L5/6 Segment		L4–6 Combined	
	Control	BMP	Control	BMP	Control	BMP
NIAD	0.95	0.58	0.885	0.722	0.724	0.58
Fusion Assessments						
Palpation	1	0.285	1	0.458	#	#
XR-Graded	1	0.473	1	0.433	#	#
XR-Categorical	1	0.066	1	1	#	#
Osteogenesis Quantifications						
XR-axitron	1	0.019 *	0.317	0.567	0.317	0.058
Micro-CT	#	#	#	#	0.806	0.327
Stiffness Measurements were for the L4–6 Combined Segment						
Stiffness Assessments		IVAD		Four-Point Bending		
Direction	Control	BMP	Control	BMP	Control	BMP
Extension	0.001 *	0.622	0.88	0.291		
Flexion	0.023 *	0.622	0.174	0.159		
Left	0.001 *	0.364	0.131	0.65		
Right	0.131	0.291	0.112	0.481		
Coronal	0.002 *	0.496	#	#		
Sagittal	0.001 *	0.573	#	#		

A comparison was made between multimodally assessed outcomes at lumbar level 4/5 (L4/5), lumbar 5/6 (L5/6) and these levels combined (L4–6) at 12 weeks following intradiscal injection of bone marrow stromal cells that were either negative control cells, or gene-programmed to express bone morphogenetic protein (BMP) BMP2/BMP7 heterodimers. Assessments were performed as described in Materials and Methods, prior data was from Cunningham et al (2022). Asterisk (*) denotes significant differences $p \leq 0.05$ were observed in the comparisons, hashtag (#) indicates inability to make the comparison. The systematic differences observed for the IVAD negative control comparisons were thought due to differences in data dispersion, and the XR osteogenesis difference at L4/5 was lost when the data was not stratified by level.

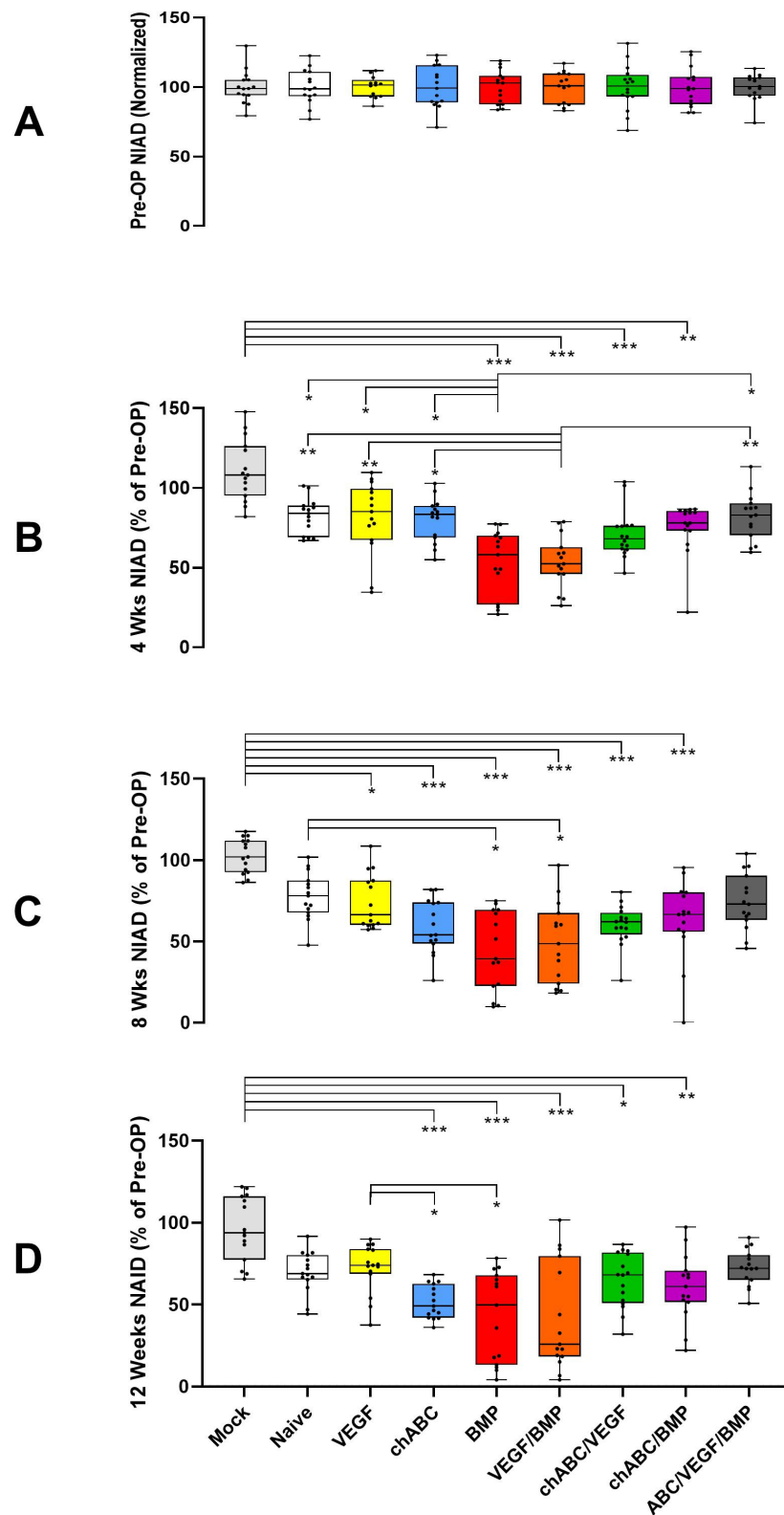


Figure A3. Coronal noninvasive angular displacement (NIAD) assessment of the L4/5 level. Time-course assessments were made: pre-operatively (A), 4 weeks post-OP (B), 8 weeks post-OP (C), and 12 weeks post-OP (D). It was expected that the BMP-containing samples would drive bone formation and cause stiffening of the spines, and that the progression of spinal stiffening would result in gradual attenuation of NIAD assessments over time. Chondroitinase ABC is abbreviated as chABC. Indicated significance: $p \leq 0.001$ (***), $p < 0.01$ (**), and $p \leq 0.05$ (*).

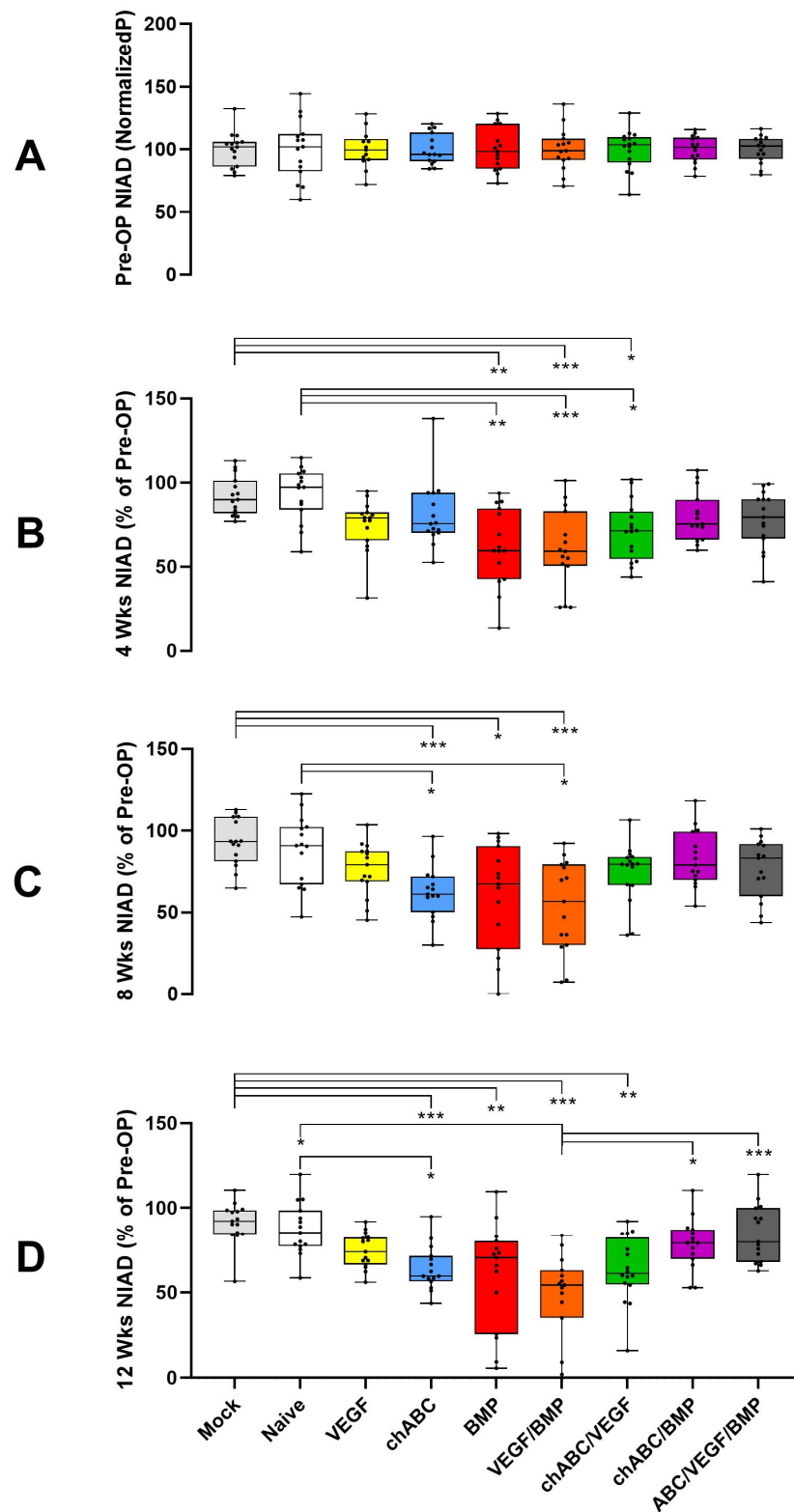


Figure A4. Coronal noninvasive angular displacement (NIAD) assessment of the L5/6 level. Time-course assessments were made: pre-operatively (A), 4 weeks post-OP (B), 8 weeks post-OP (C), and 12 weeks post-OP (D). It was expected that the BMP-containing samples would drive bone formation and cause stiffening of the spines, and that the progression of spinal stiffening would result in gradual attenuation of NIAD assessments over time. Chondroitinase ABC is abbreviated as chABC. Indicated significance: $p \leq 0.001$ (***), $p < 0.01$ (**), and $p \leq 0.05$ (*).

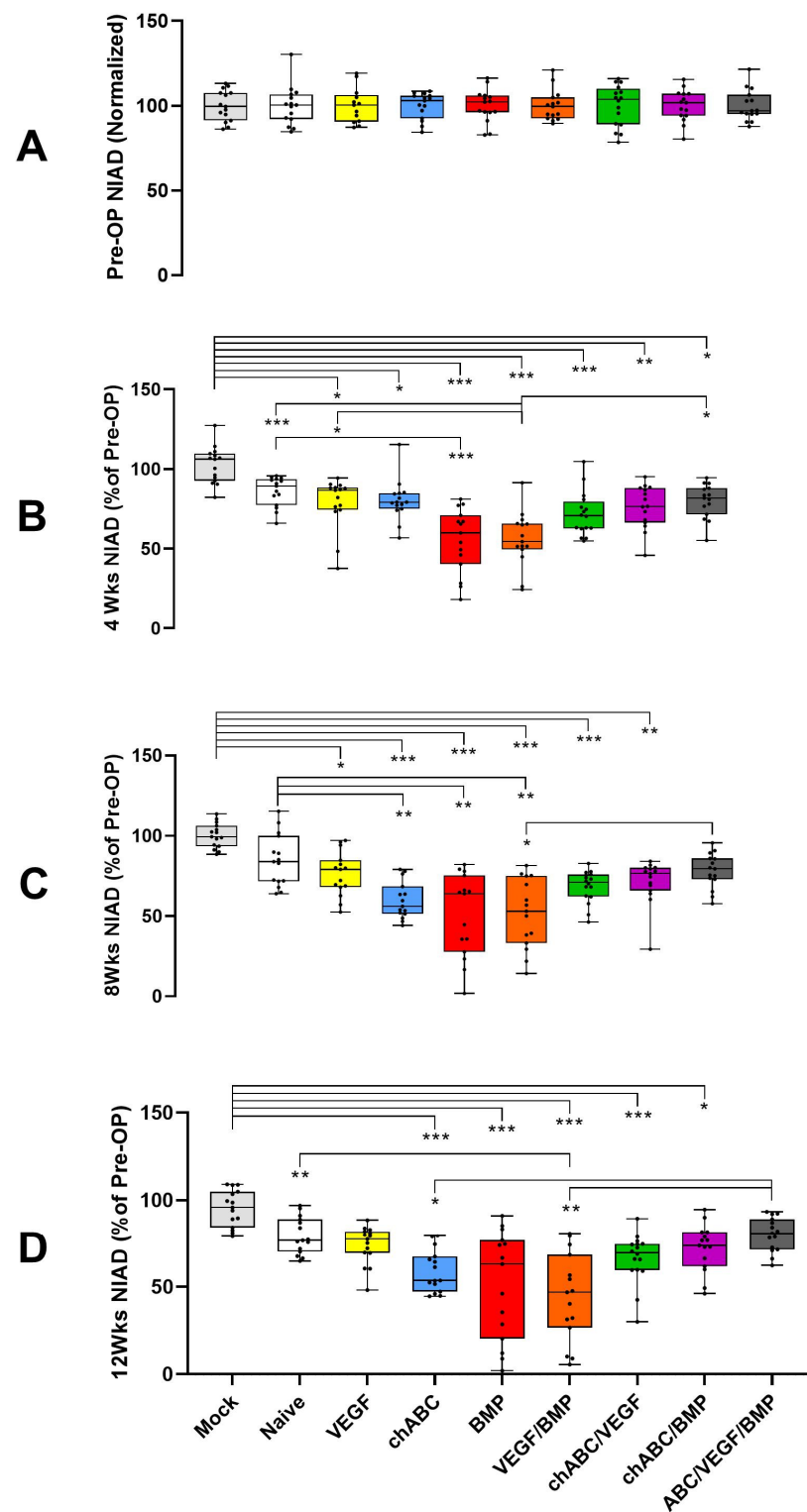


Figure A5. Coronal noninvasive angular displacement (NIAD) assessment of the L4–6 levels. Time-course assessments were made: pre-operatively (A), 4 weeks post-OP (B), 8 weeks post-OP (C), and 12 weeks post-OP (D). It was expected that the BMP-containing samples would drive bone formation and cause stiffening of the spines, and that the progression of spinal stiffening would result in gradual attenuation of NIAD assessments over time. Chondroitinase ABC is abbreviated as chABC. Indicated significance: $p \leq 0.001$ (***), $p < 0.01$ (**), and $p \leq 0.05$ (*).

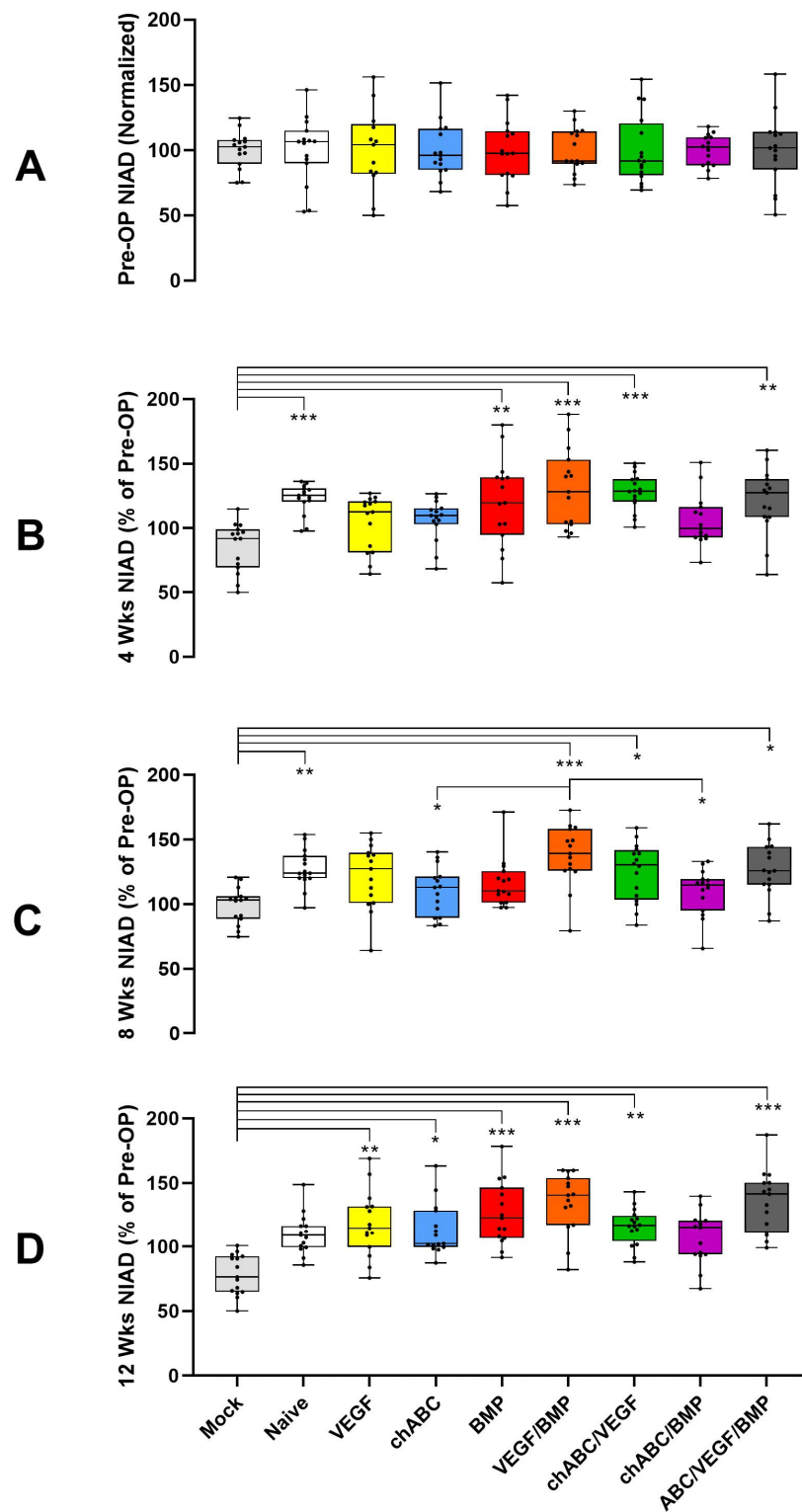


Figure A6. Coronal noninvasive angular displacement (NIAD) assessment of the L6/S1 level. Time-course assessments were made: pre-operatively (A), 4 weeks post-OP (B), 8 weeks post-OP (C), and 12 weeks post-OP (D). Due to progressive stiffening and fusion of the L4–6 segments, the L6/S1 segment was expected to become more mobile. Chondroitinase ABC is abbreviated as chABC. Indicated significance: $p \leq 0.001$ (***), $p < 0.01$ (**), and $p \leq 0.05$ (*).

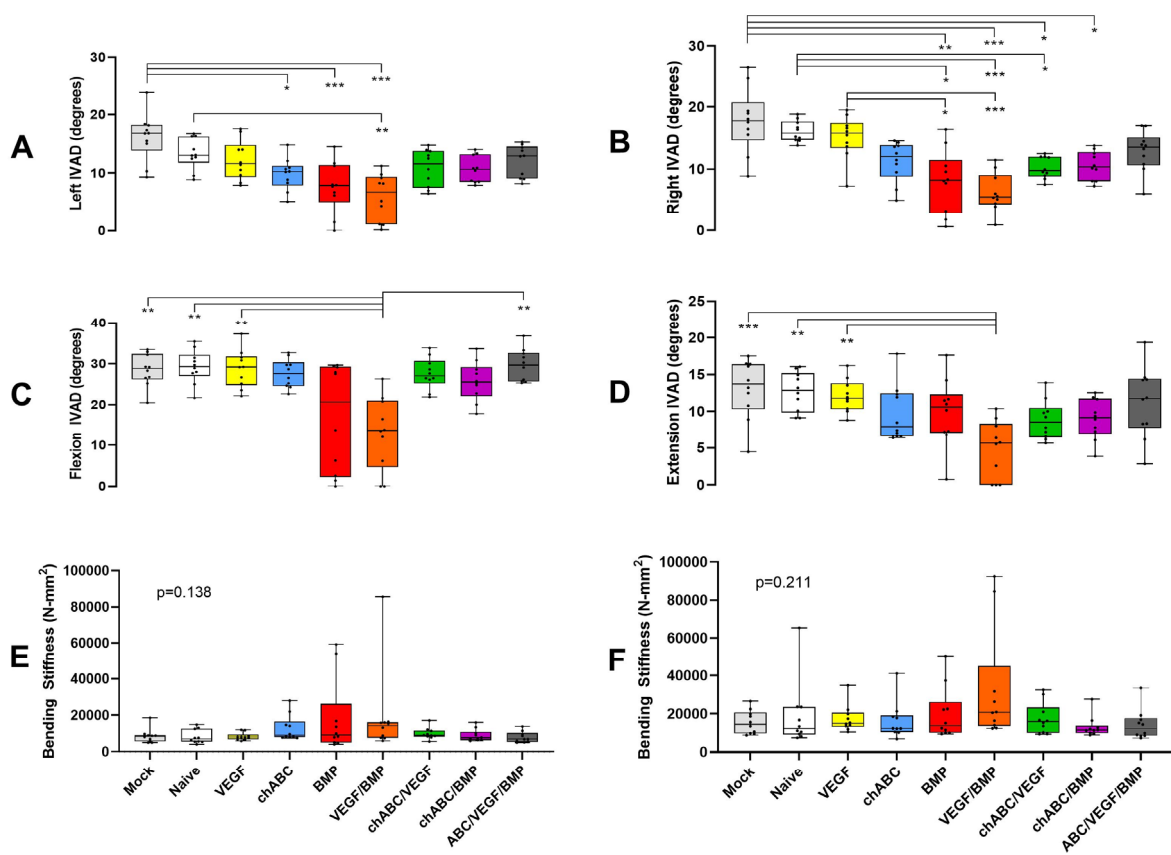


Figure A7. In vitro angular displacement (IVAD) and four-point bending assessments at 12 weeks after treatment delivery. Stiffness assessments were made over the combined L4–6 segment and were organized as: IVAD left bending (A), IVAD right bending (B), IVAD flexion (C), IVAD extension (D), 4-point bending flexion (E), and 4-point bending extension (F). Chondroitinase ABC is abbreviated as chABC. Indicated significance: $p \leq 0.001$ (***), $p < 0.01$ (**), and $p \leq 0.05$ (*).

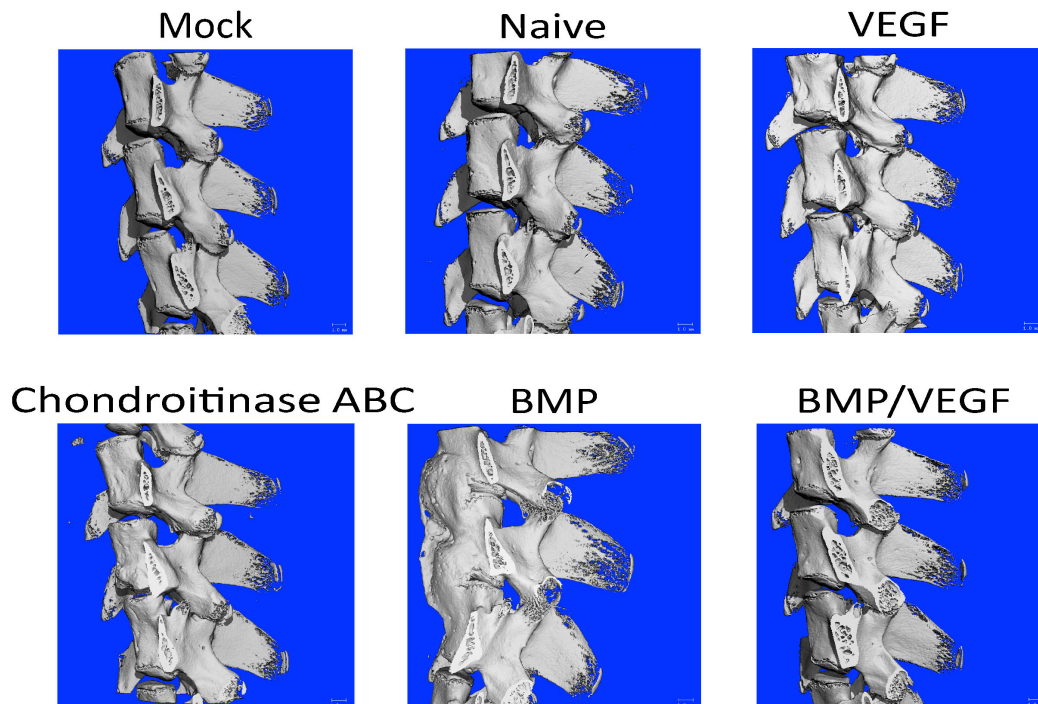


Figure A8. Cont.

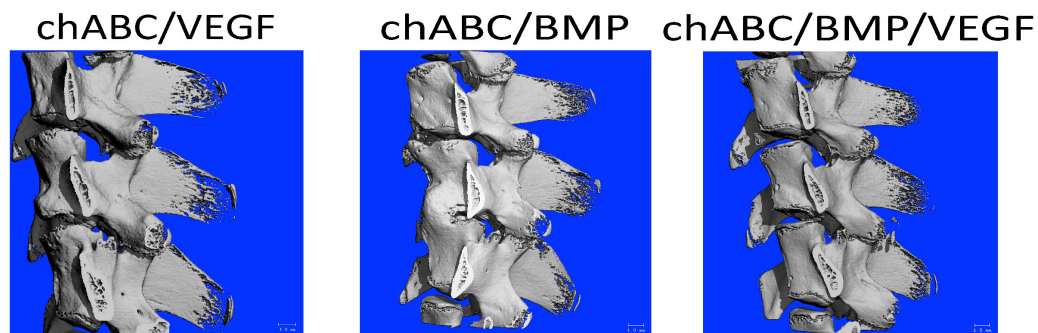


Figure A8. Selected micro-CT 3-dimensional isosurface renderings demonstrating bone induction. All samples are oriented caudal at the top, cranial at the bottom, ventral to left and dorsal to right, with vertebral L6-L4 represented top to bottom, and the scale marking in the lower right corner representing 1mm. Micro-CT assessment was performed at 12 weeks after treatment delivery. Chondroitinase ABC is abbreviated as chABC. Note induced bone causing fusion for both levels of the BMP-treated sample and for the L4/5 level of the chABC/BMP treated sample. Also note that despite the BMP/VEGF treatment group showing excellent bone production overall, the sample shown here did not produce bone at either level implanted.

References

1. Kuo, C.C.; Soliman, M.A.R.; Aguirre, A.O.; Youngs, D.; Kruk, M.; Hess, R.M.; Nyabuto, E.M.; Khan, A.; Jowdy, P.K.; Pollina, J.; et al. Risk factors of early complications after thoracic and lumbar spinal deformity surgery: A systematic review and meta-analysis. *Eur. Spine J.* **2023**, *32*, 899–913. [[CrossRef](#)] [[PubMed](#)]
2. Smith, J.S.; Klineberg, E.; Lafage, V.; Shaffrey, C.I.; Schwab, F.; Lafage, R.; Hostin, R.; Mundis, G.M., Jr.; Errico, T.J.; Kim, H.J.; et al. Prospective multicenter assessment of perioperative and minimum 2-year postoperative complication rates associated with adult spinal deformity surgery. *J. Neurosurg. Spine* **2016**, *25*, 1–14. [[CrossRef](#)] [[PubMed](#)]
3. Alhammoud, A.; Alborn, Y.; Baco, A.M.; Othman, Y.A.; Ogura, Y.; Steinhaus, M.; Sheha, E.D.; Qureshi, S.A. Minimally Invasive Scoliosis Surgery Is a Feasible Option for Management of Idiopathic Scoliosis and Has Equivalent Outcomes to Open Surgery: A Meta-Analysis. *Glob. Spine J.* **2022**, *12*, 483–492. [[CrossRef](#)]
4. Skovrlj, B.; Belton, P.; Zarzour, H.; Qureshi, S.A. Perioperative outcomes in minimally invasive lumbar spine surgery: A systematic review. *World J. Orthop.* **2015**, *6*, 996–1005. [[CrossRef](#)] [[PubMed](#)]
5. Alden, T.D.; Pittman, D.D.; Beres, E.J.; Hankins, G.R.; Kallmes, D.F.; Wisotsky, B.M.; Kerns, K.M.; Helm, G.A. Percutaneous spinal fusion using bone morphogenetic protein-2 gene therapy. *J. Neurosurg.* **1999**, *90*, 109–114. [[CrossRef](#)] [[PubMed](#)]
6. Laurent, J.J.; Webb, K.M.; Beres, E.J.; McGee, K.; Li, J.; van Rietbergen, B.; Helm, G.A. The use of bone morphogenetic protein-6 gene therapy for percutaneous spinal fusion in rabbits. *J. Neurosurg. Spine* **2004**, *1*, 90–94. [[CrossRef](#)]
7. Cunningham, M.E.; Kelly, N.H.; Rawlins, B.A.; Boachie-Adjei, O.; van der Meulen, M.C.H.; Hidaka, C. Lumbar spine intervertebral disc gene delivery of BMPs induces anterior spine fusion in lewis rats. *Sci. Rep.* **2022**, *12*, 16847. [[CrossRef](#)]
8. Kato, F.; Iwata, H.; Murakami, H.; Mimatsu, K.; Miura, T. Chemonucleolysis and response of postchemonucleolytic intervertebral disc to bone morphogenetic protein (BMP). *Rinsho Seikeigeka* **1987**, *22*, 965.
9. Kato, F. Experimental study of chemical spinal fusion in the rabbit by means of bone morphogenetic protein. *Nihon Seikeigeka Gakkai Zasshi* **1990**, *64*, 442–452.
10. Muschik, M.; Schlenzka, D.; Ritsila, V.; Tennstedt, C.; Lewandrowski, K.U. Experimental anterior spine fusion using bovine bone morphogenetic protein: A study in rabbits. *J. Orthop. Sci.* **2000**, *5*, 165–170. [[CrossRef](#)]
11. Nordby, E.J.; Wright, P.H.; Schofield, S.R. Safety of chemonucleolysis. Adverse effects reported in the United States, 1982–1991. *Clin. Orthop. Relat. Res.* **1993**, *293*, 122–134. [[CrossRef](#)]
12. Herkowitz, H.N. Current status of percutaneous discectomy and chemonucleolysis. *Orthop. Clin. N. Am.* **1991**, *22*, 327–332. [[CrossRef](#)]
13. Kato, F.; Mimatsu, K.; Iwata, H.; Miura, T. Comparison of tissue reaction with chondroitinase ABC and chymopapain in rabbits as the basis of clinical application in chemonucleolysis. *Clin. Orthop. Relat. Res.* **1993**, 294–302. [[CrossRef](#)]
14. Olmarker, K.; Danielsen, N.; Nannmark, U.; Sennerby, L.; Rydevik, B. Microvascular effects of chondroitinase ABC and chymopapain. An in vivo experimental study on hamsters and rabbits. *Clin. Orthop. Relat. Res.* **1990**, *257*, 274–279. [[CrossRef](#)]
15. Park, J.S.; Ahn, J.I. The effect of chondroitinase ABC on rabbit intervertebral disc. Radiological, histological and electron microscopic findings. *Int. Orthop.* **1995**, *19*, 103–109. [[CrossRef](#)]
16. Olmarker, K.; Stromberg, J.; Blomquist, J.; Zachrisson, P.; Nannmark, U.; Nordborg, C.; Rydevik, B. Chondroitinase ABC (pharmaceutical grade) for chemonucleolysis. Functional and structural evaluation after local application on intraspinal nerve structures and blood vessels. *Spine* **1996**, *21*, 1952–1956. [[CrossRef](#)]

17. Boxberger, J.I.; Sen, S.; Yerramalli, C.S.; Elliott, D.M. Nucleus pulposus glycosaminoglycan content is correlated with axial mechanics in rat lumbar motion segments. *J. Orthop. Res.* **2006**, *24*, 1906–1915. [[CrossRef](#)]
18. Boxberger, J.I.; Auerbach, J.D.; Sen, S.; Elliott, D.M. An in vivo model of reduced nucleus pulposus glycosaminoglycan content in the rat lumbar intervertebral disc. *Spine* **2008**, *33*, 146–154. [[CrossRef](#)]
19. He, M.; Pang, J.; Sun, H.; Zheng, G.; Lin, Y.; Ge, W. Overexpression of TIMP3 inhibits discogenic pain by suppressing angiogenesis and the expression of substance P in nucleus pulposus. *Mol. Med. Rep.* **2020**, *21*, 1163–1171. [[CrossRef](#)]
20. Tolofari, S.K.; Richardson, S.M.; Freemont, A.J.; Hoyland, J.A. Expression of semaphorin 3A and its receptors in the human intervertebral disc: Potential role in regulating neural ingrowth in the degenerate intervertebral disc. *Arthritis Res. Ther.* **2010**, *12*, R1. [[CrossRef](#)]
21. Iruela-Arispe, M.L.; Liska, D.J.; Sage, E.H.; Bornstein, P. Differential expression of thrombospondin 1, 2, and 3 during murine development. *Dev. Dyn.* **1993**, *197*, 40–56. [[CrossRef](#)] [[PubMed](#)]
22. Ishii, Y.; Thomas, A.O.; Guo, X.E.; Hung, C.T.; Chen, F.H. Localization and distribution of cartilage oligomeric matrix protein in the rat intervertebral disc. *Spine* **2006**, *31*, 1539–1546. [[CrossRef](#)] [[PubMed](#)]
23. Kusafuka, K.; Hiraki, Y.; Shukunami, C.; Kayano, T.; Takemura, T. Cartilage-specific matrix protein, chondromodulin-I (ChM-I), is a strong angio-inhibitor in endochondral ossification of human neonatal vertebral tissues in vivo: Relationship with angiogenic factors in the cartilage. *Acta Histochem.* **2002**, *104*, 167–175. [[CrossRef](#)] [[PubMed](#)]
24. Minogue, B.M.; Richardson, S.M.; Zeef, L.A.; Freemont, A.J.; Hoyland, J.A. Transcriptional profiling of bovine intervertebral disc cells: Implications for identification of normal and degenerate human intervertebral disc cell phenotypes. *Arthritis Res. Ther.* **2010**, *12*, R22. [[CrossRef](#)]
25. Li, Y.; Zhang, T.; Tian, W.; Hu, H.; Xin, Z.; Ma, X.; Ye, C.; Hang, K.; Han, X.; Zhao, J.; et al. Loss of TIMP3 expression induces inflammation, matrix degradation, and vascular ingrowth in nucleus pulposus: A new mechanism of intervertebral disc degeneration. *FASEB J.* **2020**, *34*, 5483–5498. [[CrossRef](#)]
26. Lin, D.; Alberton, P.; Delgado Caceres, M.; Prein, C.; Clausen-Schaumann, H.; Dong, J.; Aszodi, A.; Shukunami, C.; Iatridis, J.C.; Docheva, D. Loss of tenomodulin expression is a risk factor for age-related intervertebral disc degeneration. *Aging Cell* **2020**, *19*, e13091. [[CrossRef](#)]
27. Fournier, D.E.; Kiser, P.K.; Shoemaker, J.K.; Battie, M.C.; Seguin, C.A. Vascularization of the human intervertebral disc: A scoping review. *JOR Spine* **2020**, *3*, e1123. [[CrossRef](#)]
28. Kim, J.H.; Ham, C.H.; Kwon, W.K. Current Knowledge and Future Therapeutic Prospects in Symptomatic Intervertebral Disc Degeneration. *Yonsei Med. J.* **2022**, *63*, 199–210. [[CrossRef](#)]
29. Binch, A.L.; Cole, A.A.; Breakwell, L.M.; Michael, A.L.; Chiverton, N.; Cross, A.K.; Le Maitre, C.L. Expression and regulation of neurotrophic and angiogenic factors during human intervertebral disc degeneration. *Arthritis Res. Ther.* **2014**, *16*, 416. [[CrossRef](#)]
30. Chen, Q.; Wang, J.; Xia, Q.; Wu, L.; Chen, F.; Li, L.; Zhu, C.; He, M.; Jiang, Y.; Huang, Y.; et al. Treatment outcomes of injectable thermosensitive hydrogel containing bevacizumab in intervertebral disc degeneration. *Front. Bioeng. Biotechnol.* **2022**, *10*, 976706. [[CrossRef](#)]
31. Fujita, N.; Imai, J.; Suzuki, T.; Yamada, M.; Ninomiya, K.; Miyamoto, K.; Iwasaki, R.; Morioka, H.; Matsumoto, M.; Chiba, K.; et al. Vascular endothelial growth factor-A is a survival factor for nucleus pulposus cells in the intervertebral disc. *Biochem. Biophys. Res. Commun.* **2008**, *372*, 367–372. [[CrossRef](#)]
32. Rodrigues-Pinto, R.; Ward, L.; Humphreys, M.; Zeef, L.A.H.; Berry, A.; Hanley, K.P.; Hanley, N.; Richardson, S.M.; Hoyland, J.A. Human notochordal cell transcriptome unveils potential regulators of cell function in the developing intervertebral disc. *Sci. Rep.* **2018**, *8*, 12866. [[CrossRef](#)]
33. Sakai, D.; Nakai, T.; Mochida, J.; Alini, M.; Grad, S. Differential phenotype of intervertebral disc cells: Microarray and immunohistochemical analysis of canine nucleus pulposus and anulus fibrosus. *Spine* **2009**, *34*, 1448–1456. [[CrossRef](#)]
34. Agrawal, A.; Gajghate, S.; Smith, H.; Anderson, D.G.; Albert, T.J.; Shapiro, I.M.; Risbud, M.V. Cited2 modulates hypoxia-inducible factor-dependent expression of vascular endothelial growth factor in nucleus pulposus cells of the rat intervertebral disc. *Arthritis Rheum.* **2008**, *58*, 3798–3808. [[CrossRef](#)] [[PubMed](#)]
35. Kwon, W.K.; Moon, H.J.; Kwon, T.H.; Park, Y.K.; Kim, J.H. Influence of rabbit notochordal cells on symptomatic intervertebral disc degeneration: Anti-angiogenic capacity on human endothelial cell proliferation under hypoxia. *Osteoarthritis Cartilage.* **2017**, *25*, 1738–1746. [[CrossRef](#)]
36. Merceron, C.; Mangiavini, L.; Robling, A.; Wilson, T.L.; Giaccia, A.J.; Shapiro, I.M.; Schipani, E.; Risbud, M.V. Loss of HIF-1alpha in the notochord results in cell death and complete disappearance of the nucleus pulposus. *PLoS ONE* **2014**, *9*, e110768. [[CrossRef](#)] [[PubMed](#)]
37. Wu, W.J.; Zhang, X.K.; Zheng, X.F.; Yang, Y.H.; Jiang, S.D.; Jiang, L.S. SHH-dependent knockout of HIF-1 alpha accelerates the degenerative process in mouse intervertebral disc. *Int. J. Immunopathol. Pharmacol.* **2013**, *26*, 601–609. [[CrossRef](#)] [[PubMed](#)]
38. Meng, X.; Zhuang, L.; Wang, J.; Liu, Z.; Wang, Y.; Xiao, D.; Zhang, X. Hypoxia-inducible factor (HIF)-1alpha knockout accelerates intervertebral disc degeneration in mice. *Int. J. Clin. Exp. Pathol.* **2018**, *11*, 548–557.
39. Bouletreau, P.J.; Warren, S.M.; Spector, J.A.; Peled, Z.M.; Gerrets, R.P.; Greenwald, J.A.; Longaker, M.T. Hypoxia and VEGF up-regulate BMP-2 mRNA and protein expression in microvascular endothelial cells: Implications for fracture healing. *Plast. Reconstr. Surg.* **2002**, *109*, 2384–2397. [[CrossRef](#)]

40. Dai, J.; Kitagawa, Y.; Zhang, J.; Yao, Z.; Mizokami, A.; Cheng, S.; Nor, J.; McCauley, L.K.; Taichman, R.S.; Keller, E.T. Vascular endothelial growth factor contributes to the prostate cancer-induced osteoblast differentiation mediated by bone morphogenetic protein. *Cancer Res.* **2004**, *64*, 994–999. [[CrossRef](#)]
41. Li, G.; Cui, Y.; McMurray, L.; Allen, W.E.; Wang, H. rhBMP-2, rhVEGF(165), rhPTN and thrombin-related peptide, TP508 induce chemotaxis of human osteoblasts and microvascular endothelial cells. *J. Orthop. Res.* **2005**, *23*, 680–685. [[CrossRef](#)] [[PubMed](#)]
42. Peng, H.; Wright, V.; Usas, A.; Gearhart, B.; Shen, H.C.; Cummins, J.; Huard, J. Synergistic enhancement of bone formation and healing by stem cell-expressed VEGF and bone morphogenetic protein-4. *J. Clin. Investig.* **2002**, *110*, 751–759. [[CrossRef](#)] [[PubMed](#)]
43. Peng, H.; Usas, A.; Olshanski, A.; Ho, A.M.; Gearhart, B.; Cooper, G.M.; Huard, J. VEGF improves, whereas sFlt1 inhibits, BMP2-induced bone formation and bone healing through modulation of angiogenesis. *J. Bone Miner. Res.* **2005**, *20*, 2017–2027. [[CrossRef](#)] [[PubMed](#)]
44. Damle, S.R.; Rawlins, B.A.; Boachie-Adjei, O.; Crystal, R.G.; Hidaka, C.; Cunningham, M.E. Lumbar spine intervertebral disc gene delivery: A pilot study in lewis rats. *HSS J.* **2013**, *9*, 36–41. [[CrossRef](#)]
45. Damle, S.R.; Krzyzanowska, A.; Frawley, R.J.; Cunningham, M.E. Surgical anatomy, transperitoneal approach, and early postoperative complications of a ventral lumbar spine surgical model in Lewis rats. *Comp. Med.* **2013**, *63*, 409–415.
46. Cunningham, M.E.; Beach, J.M.; Bilgic, S.; Boachie-Adjei, O.; van der Meulen, M.C.; Hidaka, C. In vivo and in vitro analysis of rat lumbar spine mechanics. *Clin. Orthop. Relat. Res.* **2010**, *468*, 2695–2703. [[CrossRef](#)]
47. Bae, H.W.; Zhao, L.; Kanim, L.E.; Wong, P.; Marshall, D.; Delamarter, R.B. Bone marrow enhances the performance of rhBMP-2 in spinal fusion: A rodent model. *J. Bone Jt. Surg. Am.* **2013**, *95*, 338–347. [[CrossRef](#)]
48. Peterson, B.; Whang, P.G.; Iglesias, R.; Wang, J.C.; Lieberman, J.R. Osteoinductivity of commercially available demineralized bone matrix. Preparations in a spine fusion model. *J. Bone Jt. Surg. Am.* **2004**, *86*, 2243–2250. [[CrossRef](#)]
49. Melgoza, I.P.; Chenna, S.S.; Tessier, S.; Zhang, Y.; Tang, S.Y.; Ohnishi, T.; Novais, E.J.; Kerr, G.J.; Mohanty, S.; Tam, V.; et al. Development of a standardized histopathology scoring system using machine learning algorithms for intervertebral disc degeneration in the mouse model—An ORS spine section initiative. *JOR Spine* **2021**, *4*, e1164. [[CrossRef](#)]
50. Mohd Isa, I.L.; Abbah, S.A.; Kilcoyne, M.; Sakai, D.; Dockery, P.; Finn, D.P.; Pandit, A. Implantation of hyaluronic acid hydrogel prevents the pain phenotype in a rat model of intervertebral disc injury. *Sci. Adv.* **2018**, *4*, eaaq0597. [[CrossRef](#)]
51. Yaniv, G.; Bader, S.; Lidar, M.; Herman, A.; Shazar, N.; Aharoni, D.; Eshed, I. The natural course of bridging osteophyte formation in diffuse idiopathic skeletal hyperostosis: Retrospective analysis of consecutive CT examinations over 10 years. *Rheumatology* **2014**, *53*, 1951–1957. [[CrossRef](#)] [[PubMed](#)]
52. Krzyzanowska, A.K.; Frawley, R.J.; Damle, S.; Chen, T.; Otero, M.; Cunningham, M.E. Activation of nuclear factor-kappa B by TNF promotes nucleus pulposus mineralization through inhibition of ANKH and ENPP1. *Sci. Rep.* **2021**, *11*, 8271. [[CrossRef](#)] [[PubMed](#)]
53. Cunningham, M.E.; Greene, L.A. A function-structure model for NGF-activated TRK. *EMBO J.* **1998**, *17*, 7282–7293. [[CrossRef](#)]
54. Cunningham, M.E.; Stephens, R.M.; Kaplan, D.R.; Greene, L.A. Autophosphorylation of activation loop tyrosines regulates signaling by the TRK nerve growth factor receptor. *J. Biol. Chem.* **1997**, *272*, 10957–10967. [[CrossRef](#)] [[PubMed](#)]
55. Koo, T.K.; Li, M.Y. A Guideline of Selecting and Reporting Intraclass Correlation Coefficients for Reliability Research. *J. Chiropr. Med.* **2016**, *15*, 155–163. [[CrossRef](#)] [[PubMed](#)]
56. Landis, J.R.; Koch, G.G. The measurement of observer agreement for categorical data. *Biometrics* **1977**, *33*, 159–174. [[CrossRef](#)]
57. Kim, J.W.; Jeon, N.; Shin, D.E.; Lee, S.Y.; Kim, M.; Han, D.H.; Shin, J.Y.; Lee, S. Regeneration in Spinal Disease: Therapeutic Role of Hypoxia-Inducible Factor-1 Alpha in Regeneration of Degenerative Intervertebral Disc. *Int. J. Mol. Sci.* **2021**, *22*, 5281. [[CrossRef](#)]
58. Risbud, M.V.; Schipani, E.; Shapiro, I.M. Hypoxic regulation of nucleus pulposus cell survival: From niche to notch. *Am. J. Pathol.* **2010**, *176*, 1577–1583. [[CrossRef](#)]
59. Ambati, B.K.; Nozaki, M.; Singh, N.; Takeda, A.; Jani, P.D.; Suthar, T.; Albuquerque, R.J.; Richter, E.; Sakurai, E.; Newcomb, M.T.; et al. Corneal avascularity is due to soluble VEGF receptor-1. *Nature* **2006**, *443*, 993–997. [[CrossRef](#)]
60. Capossela, S.; Bertolo, A.; Gunasekera, K.; Potzel, T.; Baur, M.; Stoyanov, J.V. VEGF vascularization pathway in human intervertebral disc does not change during the disc degeneration process. *BMC Res. Notes* **2018**, *11*, 333. [[CrossRef](#)]
61. Carreon, L.Y.; Ito, T.; Yamada, M.; Uchiyama, S.; Takahashi, H.; Ikuta, F. Histologic changes in the disc after cervical spine trauma: Evidence of disc absorption. *J. Spinal Disord.* **1996**, *9*, 313–316. [[CrossRef](#)] [[PubMed](#)]
62. Foulsham, W.; Dohlman, T.H.; Mittal, S.K.; Taketani, Y.; Singh, R.B.; Masli, S.; Dana, R. Thrombospondin-1 in ocular surface health and disease. *Ocul. Surf.* **2019**, *17*, 374–383. [[CrossRef](#)] [[PubMed](#)]
63. Cursiefen, C.; Masli, S.; Ng, T.F.; Dana, M.R.; Bornstein, P.; Lawler, J.; Streilein, J.W. Roles of thrombospondin-1 and -2 in regulating corneal and iris angiogenesis. *Investig. Ophthalmol. Vis. Sci.* **2004**, *45*, 1117–1124. [[CrossRef](#)]
64. Tucker, R.P.; Hagios, C.; Chiquet-Ehrismann, R.; Lawler, J. In situ localization of thrombospondin-1 and thrombospondin-3 transcripts in the avian embryo. *Dev. Dyn.* **1997**, *208*, 326–337. [[CrossRef](#)]
65. Ebrahim, Q.; Qi, J.H.; Sugimoto, M.; Ali, M.; Sears, J.E.; Cutler, A.; Khokha, R.; Vasanji, A.; Anand-Apte, B. Increased neovascularization in mice lacking tissue inhibitor of metalloproteinases-3. *Investig. Ophthalmol. Vis. Sci.* **2011**, *52*, 6117–6123. [[CrossRef](#)] [[PubMed](#)]

66. Ma, D.H.; Zhang, F.; Shi, W.; Yao, J.Y.; Hsiao, C.H.; Wu, H.C.; Kim, W.S.; Hao, Y.X.; Hwang, D.G.; Chen, J.K.; et al. Expression of tissue inhibitor of metalloproteinase-4 in normal human corneal cells and experimental corneal neovascularization. *Ophthalmic Res.* **2003**, *35*, 199–207. [[CrossRef](#)]
67. Azar, D.T. Corneal angiogenic privilege: Angiogenic and antiangiogenic factors in corneal avascularity, vasculogenesis, and wound healing (an American Ophthalmological Society thesis). *Trans. Am. Ophthalmol. Soc.* **2006**, *104*, 264–302.
68. Barry, Z.; Park, B.; Corson, T.W. Pharmacological Potential of Small Molecules for Treating Corneal Neovascularization. *Molecules* **2020**, *25*, 3468. [[CrossRef](#)]
69. Gutman, G.; Barak, V.; Maslovitz, S.; Amit, A.; Lessing, J.B.; Geva, E. Regulation of vascular endothelial growth factor-A and its soluble receptor sFlt-1 by luteinizing hormone in vivo: Implication for ovarian follicle angiogenesis. *Fertil. Steril.* **2008**, *89*, 922–926. [[CrossRef](#)]
70. Ku, C.H.; White, K.E.; Dei Cas, A.; Hayward, A.; Webster, Z.; Bilous, R.; Marshall, S.; Viberti, G.; Gnudi, L. Inducible overexpression of sFlt-1 in podocytes ameliorates glomerulopathy in diabetic mice. *Diabetes* **2008**, *57*, 2824–2833. [[CrossRef](#)]
71. Mutter, W.P.; Karumanchi, S.A. Molecular mechanisms of preeclampsia. *Microvasc. Res.* **2008**, *75*, 1–8. [[CrossRef](#)]
72. Purpura, K.A.; George, S.H.; Dang, S.M.; Choi, K.; Nagy, A.; Zandstra, P.W. Soluble Flt-1 regulates Flk-1 activation to control hematopoietic and endothelial development in an oxygen-responsive manner. *Stem Cells* **2008**, *26*, 2832–2842. [[CrossRef](#)]
73. Shibuya, M. Vascular endothelial growth factor and its receptor system: Physiological functions in angiogenesis and pathological roles in various diseases. *J. Biochem.* **2013**, *153*, 13–19. [[CrossRef](#)] [[PubMed](#)]
74. Liao, L.; Zhao, X.; Zhou, M.; Deng, Y.; Li, Y.; Peng, C. sFlt-1: A Double Regulator in Angiogenesis-related Diseases. *Curr. Pharm. Des.* **2021**, *27*, 4160–4170. [[CrossRef](#)] [[PubMed](#)]
75. Russo, J.W.; Castellot, J.J. CCN5: Biology and pathophysiology. *J. Cell Commun. Signal.* **2010**, *4*, 119–130. [[CrossRef](#)] [[PubMed](#)]
76. Meadows, S.M.; Fletcher, P.J.; Moran, C.; Xu, K.; Neufeld, G.; Chauvet, S.; Mann, F.; Krieg, P.A.; Cleaver, O. Integration of repulsive guidance cues generates avascular zones that shape mammalian blood vessels. *Circ. Res.* **2012**, *110*, 34–46. [[CrossRef](#)]
77. Masuda, T.; Shiga, T. Chemorepulsion and cell adhesion molecules in patterning initial trajectories of sensory axons. *Neurosci. Res.* **2005**, *51*, 337–347. [[CrossRef](#)] [[PubMed](#)]
78. Reese, D.E.; Hall, C.E.; Mikawa, T. Negative regulation of midline vascular development by the notochord. *Dev. Cell* **2004**, *6*, 699–708. [[CrossRef](#)]
79. Bressan, M.; Davis, P.; Timmer, J.; Herzlinger, D.; Mikawa, T. Notochord-derived BMP antagonists inhibit endothelial cell generation and network formation. *Dev. Biol.* **2009**, *326*, 101–111. [[CrossRef](#)]
80. Rattner, A.; Yu, H.; Williams, J.; Smallwood, P.M.; Nathans, J. Endothelin-2 signaling in the neural retina promotes the endothelial tip cell state and inhibits angiogenesis. *Proc. Natl. Acad. Sci. USA* **2013**, *110*, E3830–E3839. [[CrossRef](#)]
81. Binch, A.L.; Cole, A.A.; Breakwell, L.M.; Michael, A.L.; Chiverton, N.; Creemers, L.B.; Cross, A.K.; Le Maitre, C.L. Class 3 semaphorins expression and association with innervation and angiogenesis within the degenerate human intervertebral disc. *Oncotarget* **2015**, *6*, 18338–18354. [[CrossRef](#)] [[PubMed](#)]
82. Mima, Y.; Suzuki, S.; Fujii, T.; Morikawa, T.; Tamaki, S.; Takubo, K.; Shimoda, M.; Miyamoto, T.; Watanabe, K.; Matsumoto, M.; et al. Potential involvement of semaphorin 3A in maintaining intervertebral disc tissue homeostasis. *J. Orthop. Res.* **2019**, *37*, 972–980. [[CrossRef](#)] [[PubMed](#)]
83. Murray, S.S.; Brochmann Murray, E.J.; Wang, J.C.; Duarte, M.E. The history and histology of bone morphogenetic protein. *Histol. Histopathol.* **2016**, *31*, 721–732. [[PubMed](#)]
84. Koosha, E.; Eames, B.F. Two Modulators of Skeletal Development: BMPs and Proteoglycans. *J. Dev. Biol.* **2022**, *10*, 15. [[CrossRef](#)] [[PubMed](#)]
85. Yokobori, T.; Oohira, A.; Nogami, H. Proteoglycans synthesized in calluses at various stages of fracture healing in rats. *Biochim. Biophys. Acta* **1980**, *628*, 174–181. [[CrossRef](#)]
86. Masuda, K.; Imai, Y.; Okuma, M.; Muehleman, C.; Nakagawa, K.; Akeda, K.; Thonar, E.; Andersson, G.; An, H.S. Osteogenic protein-1 injection into a degenerated disc induces the restoration of disc height and structural changes in the rabbit anular puncture model. *Spine* **2006**, *31*, 742–754. [[CrossRef](#)]
87. Miyamoto, K.; Masuda, K.; Kim, J.G.; Inoue, N.; Akeda, K.; Andersson, G.B.; An, H.S. Intradiscal injections of osteogenic protein-1 restore the viscoelastic properties of degenerated intervertebral discs. *Spine J.* **2006**, *6*, 692–703. [[CrossRef](#)]
88. Patel, S.R.; Lee, L.Y.; Mack, C.A.; Polce, D.R.; El-Sawy, T.; Hackett, N.R.; Ilcercil, A.; Jones, E.C.; Hahn, R.T.; Isom, O.W.; et al. Safety of direct myocardial administration of an adenovirus vector encoding vascular endothelial growth factor 121. *Hum. Gene Ther.* **1999**, *10*, 1331–1348. [[CrossRef](#)]
89. Kremer, E.J.; Di Falco, N.D.; Opolon, P.; Perricaudet, M. Adenovirus vector-transduced hepatocytes implanted via a preformed collagen/PTFE support persist for at least 4 weeks in vivo. *Gene Ther.* **1996**, *3*, 932–936.
90. Wu, J.C.; Sundaresan, G.; Iyer, M.; Gambhir, S.S. Noninvasive optical imaging of firefly luciferase reporter gene expression in skeletal muscles of living mice. *Mol. Ther.* **2001**, *4*, 297–306. [[CrossRef](#)]
91. Hettiaratchi, M.H.; O'Meara, M.J.; O'Meara, T.R.; Pickering, A.J.; Letko-Khait, N.; Shoichet, M.S. Reengineering biocatalysts: Computational redesign of chondroitinase ABC improves efficacy and stability. *Sci. Adv.* **2020**, *6*, eabc6378. [[CrossRef](#)]
92. Corvetti, L.; Rossi, F. Degradation of chondroitin sulfate proteoglycans induces sprouting of intact purkinje axons in the cerebellum of the adult rat. *J. Neurosci.* **2005**, *25*, 7150–7158. [[CrossRef](#)] [[PubMed](#)]

93. Kaito, T.; Johnson, J.; Ellerman, J.; Tian, H.; Aydogan, M.; Chatsrinopkun, M.; Ngo, S.; Choi, C.; Wang, J.C. Synergistic effect of bone morphogenetic proteins 2 and 7 by ex vivo gene therapy in a rat spinal fusion model. *J. Bone Jt. Surg. Am.* **2013**, *95*, 1612–1619. [[CrossRef](#)]
94. Zhu, W.; Rawlins, B.A.; Boachie-Adjei, O.; Myers, E.R.; Arimizu, J.; Choi, E.; Lieberman, J.R.; Crystal, R.G.; Hidaka, C. Combined bone morphogenetic protein-2 and -7 gene transfer enhances osteoblastic differentiation and spine fusion in a rodent model. *J. Bone Miner. Res.* **2004**, *19*, 2021–2032. [[CrossRef](#)]
95. Ferrara, N. Vascular endothelial growth factor: Basic science and clinical progress. *Endocr. Rev.* **2004**, *25*, 581–611. [[CrossRef](#)] [[PubMed](#)]
96. Owen-Woods, C.; Kusumbe, A. Fundamentals of bone vasculature: Specialization, interactions and functions. *Semin. Cell Dev. Biol.* **2022**, *123*, 36–47. [[CrossRef](#)] [[PubMed](#)]

Disclaimer/Publisher’s Note: The statements, opinions and data contained in all publications are solely those of the individual author(s) and contributor(s) and not of MDPI and/or the editor(s). MDPI and/or the editor(s) disclaim responsibility for any injury to people or property resulting from any ideas, methods, instructions or products referred to in the content.